Ore Geology Reviews 77 (2016) 163–175

Contents lists available at ScienceDirect

Ore Geology Reviews

journal homepage: www.elsevier.com/locate/oregeorev

Jurassic–Cretaceous granitoids and related tectono-metallogenesis in the Zapug–Duobuza arc, western Tibet

Quan-Ru Geng [a,*], Zhang Zhang [a], Zhi-Min Peng [a], Jun-Lei Guan [a], Xiang-Ping Zhu [a], Xiao-Chang Mao [b]

[a] Chengdu Center, China Geological Survey, Chengdu 610082, China
[b] China Geological Survey, Beijing 100037, China

ARTICLE INFO

Article history:
Received 22 November 2015
Received in revised form 22 February 2016
Accepted 25 February 2016
Available online 27 February 2016

Keywords:
Zapug–Duobuza arc
Geochemistry
South Qiangtang terrane
Metallogenesis
Tethyan evolution

ABSTRACT

The Zapug–Duobuza magmatic arc (ZDMA), located along the southern edge of the south Qiangtang terrane in western Tibet, extends east–west for ~400 km. Small scattered granite and porphyry intrusions crop out in the ZDMA, but a large amount of granite may be buried by Late Cretaceous to Paleogene thrusting. Two stages of magmatism have been identified, at 170–150 Ma and 130–110 Ma. The widely distributed Middle–Late Jurassic granite intrusions in the ZDMA exhibit Sr—Nd isotopic characteristics similar to those of ore-bearing porphyries in the Duolong giant Cu—Au deposit, and their εHf(t) values mostly overlap those of other porphyry Cu—Mo deposits in the ZDMA and the Gangdese zone. The Sr—Nd—Hf isotopic geochemistry suggests variable contributions of mantle and Qiangtang crustal sources, and indicates the presence of two new ore districts with potentials for Cu—Au, Fe, and Pb—Zn ores, located in the Jiacuo–Liqunshan and Larelaxin–Caima areas. Except for the Duolong ore-forming porphyries, which show significant contributions of mantle components intruded into an accretionary mélange setting, the Early Cretaceous granites in other areas of the belt are of mostly crustal origin, from sources in Qiangtang felsic basement and Permo-Carboniferous strata, indicating the weak ore-forming potential of skarn-type Fe and Pb—Zn deposits. The ephemeral but deep Bangong Co–Nujiang ocean in the Early Jurassic evolved into a shallow compressional marine basin in the Middle–Late Jurassic, possibly transitioning to northward flat subduction of oceanic crust at this time. The subducted slab broke off in the Early Cretaceous, initiating a peak in arc magmatism and metallogenesis at 125–110 Ma.

1. Introduction

As part of the eastern Tethyan metallogenic domain, the Tibetan Plateau includes two well-documented metallogenic belts, the Gangdese metallogenic zone in southern Tibet, which is mainly related to continental collision, and the newly delimited Bangong Co–Nujiang metallogenic belt (BNM) in central Tibet, which is related to an accretionary orogen (Hou and Zhang, 2015; Hou et al., 2015; Richards, 2015). The BNM, which has received significant attention during recent geological and mineral surveys, is composed of three subzones: the southern Qiangtang terrane, the Bangong Co–Nujiang suture zone (BNS), and the northern Gangdese magmatic arc (referred to as the "northern Lhasa subterrane" by Zhu et al., 2015a) (Fig. 1A). Mineralization in the BNM, which is concentrated mainly in magmatic arcs to the north and south of the BNS (Geng et al., 2013), is related to bidirectional subduction of the BNS Tethyan Ocean crust during the Middle Jurassic–Cretaceous (Li et al., 2014a,b,c; Zhu et al., 2015a). In addition to porphyry Cu—Au, skarn, and hydrothermal Fe—Cu—Pb—Zn deposits related to arc metallogenesis on both sides of the BNS, podiform chromite and epithermal Au deposits within the BNS also constitute major mineralization types in the BNM (Geng et al., 2011).

The Jurassic–Cretaceous Zapug–Duobuza magmatic arc (ZDMA), located along the southern margin of the south Qiangtang terrane, was first identified during regional geological mapping at a scale of 1:250,000 in 2000–2005, and has been interpreted to be the result of northward subduction of BNS oceanic crust (Liu et al., 2004; Pan et al., 2004; Zhang et al., 2011; Li et al., 2014c). Ongoing geological and mineral surveys in the BNM in recent years have led to the recognition of the ore-forming potential of the ZDMA, and the demonstration of its economic significance. Major achievements of the mineral surveys of the ZDMA include the discovery of the Duolong super-large ore deposit (5.4 Mt at 0.72% Cu and 41 t at 0.23 g/t Au) (Li et al., 2014a,b; Hou and Zhang, 2015) and two ore prospecting districts in the belt. Numerous deposits and mineral occurrences have been discovered, mostly in the regions of Caima–Fuye and Duobuza–Qingcaoshan (Geng et al., 2013, 2015), leading to the establishment of the western and eastern prospecting districts in the ZDMA zone (Fig. 1B).

In-depth geological and mineral investigations of the ZDMA reveal several important problems that constrain further geological and

* Corresponding author.
E-mail address: gquanru@cgs.cn (Q.-R. Geng).

http://dx.doi.org/10.1016/j.oregeorev.2016.02.018
0169-1368/

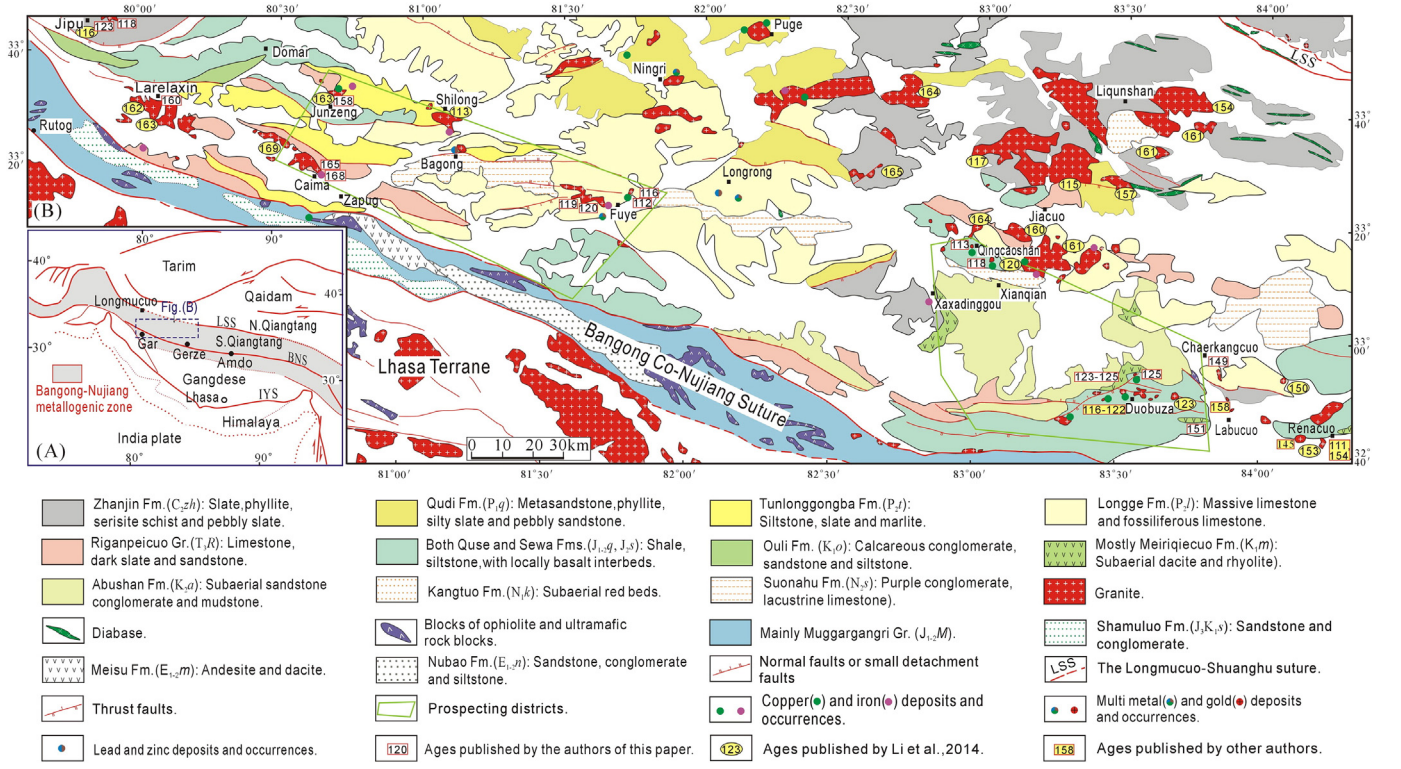

Fig. 1. (A) Tectonic framework of the Tibetan Plateau. (B) Geological map of the Zapug–Duobuza magmatic arc (modified from Geng et al., 2012b). Ore deposits and mineral occurrences are from Geng et al. (2015, 2012a) and Li et al. (2014a, 2014b), and field observations by the authors. Age data are from recent publications including Zhang et al. (2011); Geng et al. (2012a), and Li et al. (2014a).

mineral prospecting. (1) Although the ZDMA has been interpreted as the result of northward subduction of the BNS Tethys crust, an interpretation that has received increasing support in recent years (Li et al., 2014a,c, 2015; Liu et al., 2015; Zhu et al., 2015a), it is unclear why it is not a continuous zone of mostly magmatic rocks, similar to the Gangdese arc to the south. (2) The porphyry Cu—Au deposits discovered in the eastern prospecting district are Early Cretaceous in age (as discussed below); however, the ore-forming potential of the more widely distributed Middle–Late Jurassic granite intrusions in the ZDMA remains unclear. Porphyry Cu deposits in porphyritic granites emplaced into carbonate host rocks have yet to be found, with the exception of some small skarn-type deposits and occurrences, such as in the regions of Zapug–Fuye and Jiacuo–Liqunshan. Thus, the sources of granitic magma and ore-forming metals require more constraints so as to facilitate further mineral prospecting.

A 1:50,000 scale geological survey and related thematic studies in the ZDMA have been conducted since 2010, and large amounts of chronological and geochemical data have been published (e.g., Zhang et al., 2011, 2015; Geng et al., 2012a, 2015; Li et al., 2013, 2014a,b,c; Peng et al., 2015). In this paper, we present the results of a comprehensive study based on field observations, published geochemical and geochronological data, and newly obtained Rb—Sr and Sm—Nd isotope analytical results, and we discuss the geological and metallogenetic features of the ZDMA.

2. Geological setting of the ZDMA

The distribution of granitoids in the ZDMA is different to that of granitoids in the more typical Gangdese magmatic arc, although the granitoids in both regions exhibit similar origins, related to northward subduction of the BNS and Yarlung Zangbo oceanic crusts during the Jurassic–Cretaceous (Zhang et al., 2010, 2014; Zhu et al., 2015a).

2.1. Width of the magmatic zone

The ZDMA, at the southern edge of the south Qiangtang terrane in western Tibet (Fig. 1A), extends from Larelaxin, Caima, and Fuye in northern Rutog County to Duobuza in northern Gerze County (Fig. 1B). The belt is ~400 km long and trends east–west. It extends to the BNS in the south, while no distinct boundary faults have been observed to the north. The eastward extension of the belt remains unclear. In addition to the Caima, Fuye, and Duobuza ore-bearing granitic intrusions, scattered granite (porphyry) intrusions in Ningri, Liqunshan, Xianqian, and other areas close to the Longmucuo–Shuanghu suture and within the 200-km-wide south Qiangtang terrane are considered to be part of the magmatic arc (Fig. 1B) (Li et al., 2014a,c; Liu et al., 2015). According to Leloup et al. (2012), Cretaceous (117–95 Ma) mafic intrusions, basalts, diorites, dacites, and other rocks exposed to the south of Longmucuo have geochemical affinities with calc-alkaline to high-K calc-alkaline series rocks, and formed in magmatic arc and back-arc basin environments.

2.2. Atypical features of the ZDMA

The ZDMA magmatic zone is not widely exposed, unlike the magmatic zones in more typical magmatic arc belts, such as in the Gangdese and Andes belts. The zone consists of small scattered buried to semi-buried granite (porphyry) intrusions and subordinate volcanic rocks, rather than a continuous zone of magmatic rock bodies (Fig. 1B). In addition, the magmatic rocks in the ZDMA do not show distinct zonation, as they evolved over a relatively short period of time, as compared with those of the typical Gangdese arc zone, which experienced multiple stages of arc magmatism through the Permian–Cenozoic (Mo et al., 2005; Geng et al., 2009, 2011, 2013; Zhu et al., 2009, 2011a,b). However, granitic and volcanic geochemical signatures and geochronological data support the existence of a Jurassic–Cretaceous magmatic arc (Zhang

et al., 2011, 2015; Li et al., 2014a). A regional gravity anomaly map of the area displays two positive anomalies extending from the BNS to the southern Qiangtang terrane, located around Caima and Jiacuo–Duobuza (Geng et al., 2011). These suggest the existence of mafic oceanic crust that was subducted beneath the south Qiangtang terrane.

2.3. Thrust faulting and a possible hidden magmatic arc

Kapp et al. (2003a,b, 2005) and Xie et al. (2010) proposed that the south Qiangtang terrane experienced intensive tectonic thrusting during the Cretaceous–Paleogene, at which time Paleozoic strata were thrust southward over Mesozoic and Cenozoic strata for up to 70–150 km. Thrust faults were discovered in the south Qiangtang terrane during recent geological surveys and mine drilling (Fig. 2). However, the presence of a granitic zone that is hidden by the southward thrusting in the south Qiangtang terrane remains uncertain, and requires further geophysical and geological investigation.

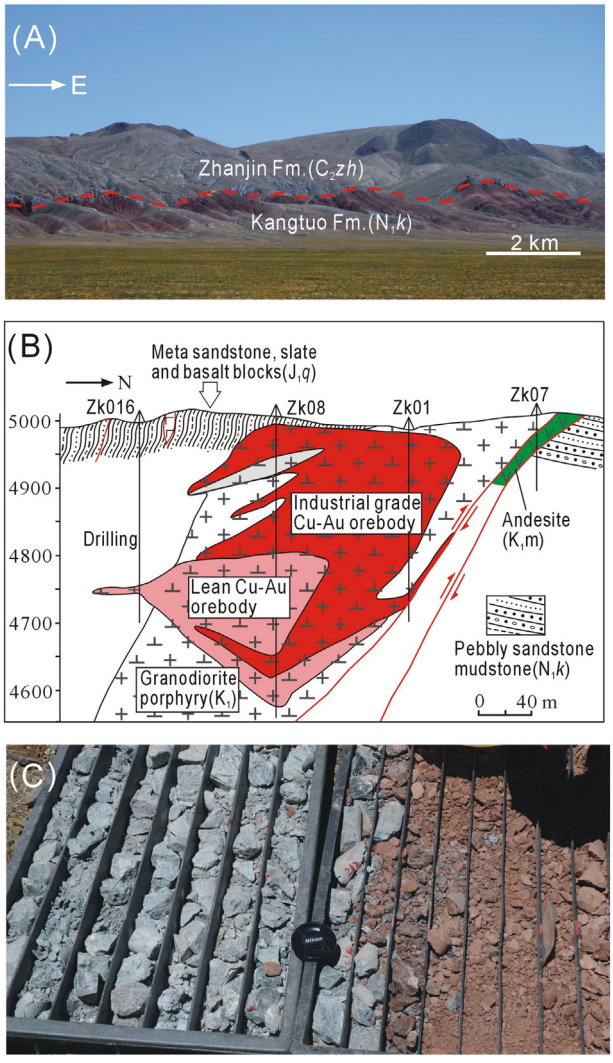

Fig. 2. Thrust faults in south Qiangtang and the Duolong deposit. (A) The Wuhuashan southward thrust south of Gangmari; see Xie et al. (2010) for a detailed geologic section and interpretation. (B) Geological and geophysical sections in Duobuza, along prospecting line No. 0 (modified from Li et al., 2012). Thick- and fine-grained Jurassic flysch sedimentary rocks, and basaltic and subordinate ultramafic rock blocks constitute an accretionary complex in the Duolong area (Li et al., 2011a). These rocks facilitated the preservation of isolated fluids and porphyry Cu—Au systems. (C) Red beds (possible N_1k strata) overthrust by Cu-mineralized porphyry (K_1), as observed in drill core from the Duobuza deposit.

2.4. Western and eastern prospecting districts

In the western prospecting district of Zapug–Fuye (Fig. 1B), Middle–Late Jurassic (169–158 Ma) and Early Cretaceous (123–112 Ma) granites intruded into fold hinges and fracture zones involving late Carboniferous–Late Triassic carbonate and clastic rocks, such as those of the Zhanjin Formation (C_2zh), Tunlonggongba Formation (P_2t), Longge Formation (P_2l), and Riganpeico Group (T_3R). The granites mainly formed skarn-type and hydrothermal deposits (Fig. 3). The Zhanjin Formation (C_2zh) is composed of medium–thick sandstone and slate beds intercalated with pebbly slate and siderite nodules, which may have provided the ore-forming metals that formed the Fe deposits. Skarn-type and hydrothermal Fe, Cu, and Pb—Zn occurrences have been discovered in Fuye, Caima, Bagong, Jiongzeng, Shilong, and other areas (Figs. 1B and 3), and are related to both Middle–Late Jurassic and Early Cretaceous granites, indicating their metallogenic potential; however, no large ore deposits have been found.

In the eastern prospecting district of Duobuza–Qingcaoshan, small shallow-seated Early Cretaceous granodiorite porphyries are intruded into a Jurassic turbidite series that includes the Quse Formation (J_1q) and the Sewa Formation (J_2s), as shown in Figs. 1B and 2B. These Jurassic formations are ductilely deformed and represent a mélange zone that differs from the typical Quse and Sewa formations in the Yanshiping Group in the northern Qiangtang terrane. A widespread penetrative shearing-related foliation and ductile folds within the Jurassic formations, coupled with tectonic blocks of basaltic pillow lavas, ultramafic rocks, and chert, have led to the recognition of fore-arc accretionary mélanges (Geng et al., 2011; Li et al., 2011a). The metallogenic age of the Duolong deposit (119–118 Ma) is slightly younger than that of the porphyry intrusions (122–118 Ma) (She et al., 2009; Zhu et al., 2011a,b). Folded Jurassic turbidites favored the formation of Cu deposits. In addition to the confirmed Duolong giant porphyry Cu—Au deposit, the Qingcaoshan and Xianqian Cu deposits, along with other deposits, have been discovered in the eastern prospecting district of Duobuza–Qingcaoshan (Li et al., 2011b, 2014a,b; Geng et al., 2013, 2015; Tang et al., 2014). Early Cretaceous hidden and shallow-seated granitic porphyries are major exploration targets for Cu—Au deposits.

3. Ages of granitoids

A large amount of geochronological data has been reported for the granite intrusions in the ZDMA. These data constrain the formation of the magmatic arc to the Middle Jurassic–Early Cretaceous (Fig. 1B); the main porphyry Cu—Au deposits formed in the Early Cretaceous.

3.1. Granitic intrusions in the Zapug–Fuye region

Several mineralized and barren granitic intrusions occur in Jipu, Larelaxin, Caima, Fuye, and other areas in the Zapug–Fuye region in the western part of the ZDMA. A monzonitic granite from the Caima intrusion yields an age of 165.1 ± 1.5 Ma, and quartz monzonite and diorite enclaves in granite yield ages of 168.3 ± 1.4 Ma and 169.5 ± 1.1 Ma, respectively (Zhang et al., 2011; Geng et al., 2012a; Li et al., 2014a). The Caima monzonitic granite intrusion yields an age of 165.1 ± 1.5 Ma, and formed a skarn-type Fe deposit. A small fine-grained quartz monzonite body from the Jiongzeng Cu occurrence north of the Caima intrusion yields an age of 158 ± 1.0 Ma (Zhang et al., 2015).

The barren Larelaxin intrusion is composed mainly of medium–coarse monzonitic granite and biotite K-feldspar granite, and yields ages of 159.40 ± 0.78 Ma, 159.96 ± 0.63 Ma, and 163–162 Ma (Zhang et al., 2011; Geng et al., 2012a; Li et al., 2014a, respectively). Age dating of a barren medium–coarse diorite granite intrusion in Jipu yields ages of 122.5 ± 2.3 Ma and 122.7 ± 3.1 Ma, and a late-stage quartz diorite porphyry yields ages of 118.27 ± 0.71 Ma and 116 ± 0.71 Ma (Li et al., 2014a).

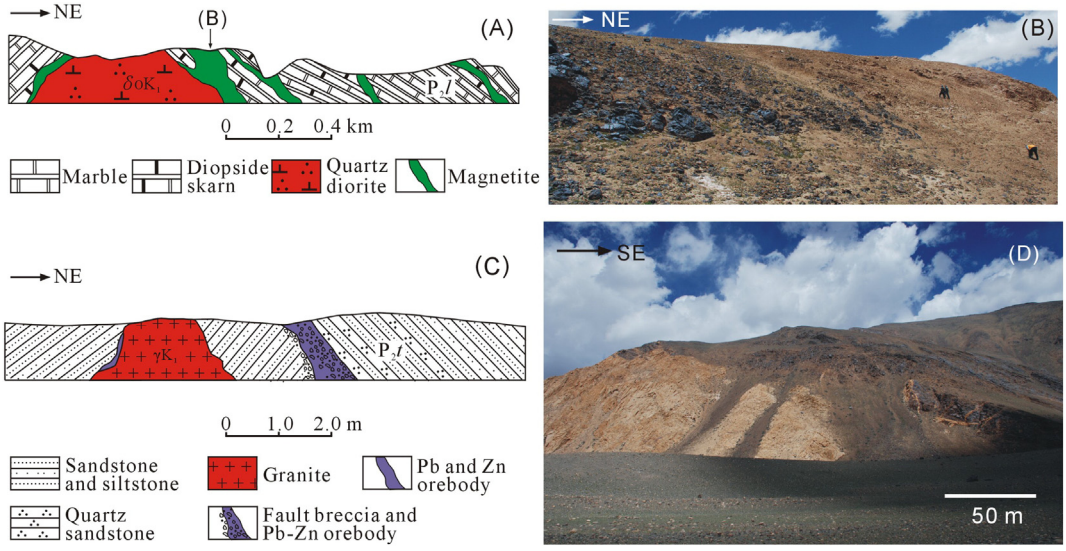

Fig. 3. Conditions of metallogenesis in the western part of the ZDMA. (A) Geological section of the Fuye magnetite deposit. Early Cretaceous quartz diorite intruded middle Permian limestone (P_2l), forming a skarn-type magnetite deposit. (B) Photograph of a magnetite ore body at Fuye. (C) Geological section of the Bagong lead–zinc deposit. Early Cretaceous granite intruded middle Permian sandstone (P_2t), resulting in hydrothermal lead–zinc mineralization in fault zones and contact zones outside the granite intrusions. (D) Clastic rocks of the Zhanjin Fm. (C_2zh) around Jipu were intruded by Early Cretaceous granite, forming a limonite alteration zone and andalusite hornfels.

The ore-forming Fuye intrusion is composed mainly of highly altered porphyraceous quartz–pyroxene monzonite, and is dated at 118.6 ± 0.73 Ma and 119.9 ± 0.56 Ma (Zhang et al., 2015). A quartz diorite intrusion near the Mushirebuka Cu occurrence to the east of the Fuye intrusion yields an age of 116.42 ± 0.59 Ma, and a dacite in this same area yields an age of 112.03 ± 0.91 Ma (Zhang et al., 2015).

These age data suggest that granitoid intrusions in the Zapug–Fuye region formed during the Middle Jurassic (169–158 Ma) and Early Cretaceous (123–112 Ma), and that both intrusive stages were related to ore-forming processes. No reliable age data have been reported for the granite intrusions in Ningri and Puge to the north, but according to regional mapping at 1:250,000 and 1:50,000 scales, they are also Middle Jurassic and Early Cretaceous in age (Pan et al., 2004).

3.2. Granitic intrusions in the Duobuza–Qingcaoshan region

Substantial progress has been made in recent years in determining the origin, style of alteration, and mineralization ages of ore-bearing and barren porphyries in the Duolong and Qingcaoshan porphyry Cu—Au deposits (Fig. 1B). These data were obtained using zircon U—Pb LA–ICP–MS (Laser Ablation Inductively Coupled Plasma Mass Spectrometry), SHRIMP (Sensitive High Resolution Ion Micro–Probe), and single-mineral $^{40}Ar/^{39}Ar$ and Re—Os analyses.

Andesites from the Meiriqiecuo Fm. in this region yield eruptive ages of 125–123 Ma, and the major Duobuza, Bolong, and Naruo ore-bearing porphyry intrusions formed at a similar time, mainly at 122–116 Ma (Qu and Xin, 2006; Zhu et al., 2011c, 2012, 2015b; Geng et al., 2012a; Chen et al., 2013; Li et al., 2013). Further studies have shown that the barren porphyries formed at 121–117 Ma, and that the ore-bearing intrusions formed at 118.6–117.5 Ma (Li et al., 2013). Molybdenite from the ore-bearing porphyries yields a Re—Os age of 118.5 ± 1.5 Ma (She et al., 2009), and altered K-feldspar yields an $^{40}Ar/^{39}Ar$ age of 119–115 Ma (Zhu et al., 2013). These data indicate that the Duolong Cu deposit formed at ca. 118 Ma, during the middle–late stage of granite porphyry intrusive activity in the Duobuza–Qingcaoshan ore district.

The Qingcaoshan and Xianqian porphyry Cu deposits, recently discovered to the north of the Duolong deposit, have intrusive ages of 112.62 ± 0.63 Ma and 117.96 ± 0.88 Ma, respectively (Geng et al., 2012a).

Some Late Jurassic granite intrusions and volcanic rocks distributed to the east of the Duobuza–Qingcaoshan district (Fig. 1B) formed at 158–145 Ma (Kapp et al., 2005; Zhang, 2007). According to the latest research, the granites in Jiacuo, Liqunshan, and Renacuo, north of the Duolong deposit, formed in the Late Jurassic (165–157 Ma) and Early Cretaceous (117–115 Ma) (Chang et al., 2011; Li et al., 2014a).

3.3. Two stages of magmatism

Geochronological data show that magmatism in the ZDMA occurred in two stages, in the Middle–Late Jurassic and Early Cretaceous; these stages are apparent in an age–frequency histogram for the magmatic rocks in the ZDMA (Fig. 4). Two peak magmatic stages, at 130–110 Ma and 170–150 Ma, are recorded in the ZDMA. A possible 10-Myr hiatus in magmatism occurred at 140–130 Ma. The distribution of ore deposits and occurrences (Fig. 1B) shows that the mineralization was related to

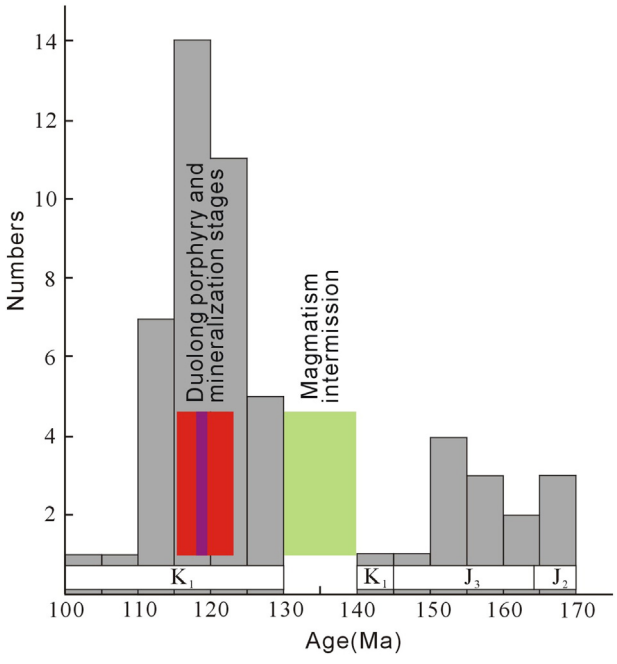

Fig. 4. Histogram of zircon U—Pb ages of granitoids in the ZDMA.

both stages of intrusion. The Duolong giant porphyry Cu deposit is clearly related to the Early Cretaceous porphyry (ca. 118 Ma), and only small-scale deposits and occurrences formed in the Middle–Late Jurassic.

4. Data sources and analytical methods

4.1. Published data

Published major and trace element data from the main granite intrusions and minor volcanic rocks in the ZDMA were used in this study. Data for the Jipu, Caima, Fuye, and other intrusions in the western section of the belt are from Zhang et al. (2011); Geng et al. (2012a), and Li et al. (2014a), and data for the Duolong and adjacent regions in the eastern section are from Li et al. (2013, 2014b); Xin et al. (2009), and Chen et al. (2013). The data are compiled in Supplementary Table 1.

Published Sr—Nd isotopic data are listed in Supplementary Table 2. The data for the Early Cretaceous Duolong metallogenic porphyry are from Zhang (2007); Xin et al. (2009); Chen et al. (2013); Li et al. (2013) and Li et al. (2014b). The data for the Late Jurassic diorite, granodiorite, and andesite in the Chaerkangcuo and Renacuo areas are from Zhang (2007).

As compared with the Sr—Nd isotopic data, considerably more zircon Hf isotope data have been reported for the ZDMA (Geng et al., 2012a; Chen et al., 2013; Li et al., 2014a,b; Zhang et al., 2015). The published zircon Hf isotopic data used in this paper are listed in Supplementary Table 3.

4.2. Analytical methods for whole-rock Rb—Sr and Sm—Nd isotopes

Based on field observations and previous studies, we performed Rb—Sr and Sm—Nd isotopic analyses on 21 samples from the main intrusions in the ZDMA. Whole-rock Sr and Nd isotope ratios were determined at the Key Laboratory of Elements and Isotopes, Guangzhou Institute of Geochemistry, Chinese Academy of Sciences, Guangzhou, China. An HF—$HClO_4$ acid dissolution method was used to digest the samples. The Rb—Sr and Sm—Nd isotopic analyses were performed on ~40 mg of whole-rock powder dissolved in Teflon bombs after being spiked with ^{87}Rb—^{84}Sr and ^{149}Sm—^{150}Nd tracers and dissolved in HF—$HClO_4$. Rb—Sr, Sm—Nd, and bulk REE were separated from other elements using a cationic resin. The Sr and Nd isotope ratios were determined using a MicroMass ISOPROBE MC–ICP–MS (Multi Collector Inductively Coupled Plasma Mass Spectrometry) instrument (for further analytical details, see Wei et al., 2002; Liang et al., 2003). The Sr and Nd isotope ratios were corrected for mass fractionation using $^{86}Sr/^{88}Sr = 0.1194$ and $^{146}Nd/^{144}Nd = 0.7219$. Standard materials measured over the course of the analysis yielded average and 2-standard deviation (SD) values of $^{87}Sr/^{86}Sr = 0.710272 \pm 0.000009$ (n = 22) for NBs987 and $^{143}Nd/^{144}Nd = 0.512112 \pm 0.000007$ (n = 26) for JNdi-1.

The Rb—Sr and Sm—Nd isotope data for the 21 samples from the main intrusions in the Zapug–Fuye zone are listed in Tables 1 and 2, respectively. These data, coupled with the published Sr—Nd isotopic data, are summarized and compared with data on a Miocene Cu-bearing porphyry from Gangdese, to evaluate the metallogenic potential of granite intrusions in the ZDMA, and their magma sources.

5. Geochemistry

5.1. Major and trace element geochemistry

The granitoid lithologies in the ZDMA are dominated by granodiorite, granite, and diorite, with subordinate quartz diorite, monzonite, and other rocks; SiO_2 contents are in the range of 55–78 wt% (Fig. 5A). On a K_2O vs. SiO_2 diagram (Fig. 5B), most samples fall into the high-K calc-alkaline and shoshonite-series fields. Samples of Early Cretaceous ore-forming porphyries of the Duolong deposit belong mostly to shoshonite-series rocks. Based on petrological and lithogeochemical studies, Li et al. (2014c) divided the Middle–Late Jurassic Larelaxin and Caima intrusions (except for mafic dikes and enclaves) into two rock groups: (1) normal calc-alkaline and shoshonitic I-type granitoids, and (2) highly fractionated I-type granitoids. These two groups can also be roughly identified throughout the ZDMA, according to SiO_2–K_2O, A/NK–A/CNK, Eu/Eu*–Differentiation Index (DI) and Harker diagrams (Figs. 5 and 6).

(1) Normal calc-alkaline and shoshonitic I-type granitoids. Most granitoid rocks in the ZDMA belong to the normal calc-alkaline and shoshonite series. As shown in Fig. 5A and B, Middle–Late Jurassic and Early Cretaceous granodiorite, quartz diorite, and granite in the eastern part of the ZDMA, around Duolong, Jiacuo and Liqunshan, are normal calc-alkaline and shoshonite-series rocks. The quartz diorite of Fuye (K_1) in the western part of the ZDMA also belongs to this group. Granitoids of this group are characterized by SiO_2 contents of 55–73 wt% and high total alkali and K_2O contents ($K_2O + Na_2O$ = 3.0–8.0 wt%; K_2O =

Table 1
Rb—Sr isotopic compositions of granitoids in ZDMA.

Sample no.	Location	Lithology	$^{87}Rb/^{86}Sr$	$^{87}Sr/^{86}Sr$	2δ	$(^{87}Sr/^{86}Sr)_i$
D1034H	N33°22′16.39″; E80°36′30.34″	Monzonitic granite	2.60	0.712932	0.000007	0.7067
D1034-2H	N33°22′20.24″; E80°36′33.20″	Monzonitic granite	2.95	0.713765	0.000008	0.7067
D1034-3H	N33°22′33.65″; E80°35′57.30″	Biotite diorite	1.74	0.711147	0.000008	0.7070
D1034-4H	N33°22′33.65″; E80°35′57.30″	Granodiorite	2.77	0.713217	0.000005	0.7066
D1035H	N33°23′3.56″; E80°34′13.76″	Granodiorite	1.92	0.711244	0.000008	0.7067
D1035-2H	N33°23′3.56″; E80°34′13.76″	Granodiorite	1.69	0.710605	0.000005	0.7065
PBN-53-3	N33°21′57.5″; E80°43′19.0″	Granite	7.58	0.720975	0.000015	0.7029
PBN-53-8	N33°21′57.5″; E80°43′19.0″	Granite	7.98	0.722763	0.000017	0.7037
PBN-54-1	N33°22′20.2″; E80°36′34.1″	Quartz monzonite	1.79	0.711811	0.000016	0.7075
D1037H	N33°27′18.23″; E80°28′4.75″	Gabbroic diorite	0.56	0.70764	0.000006	0.7063
D1039H	N33°31′36.27″; E80°09′14.86″	Granite	4.21	0.717053	0.000006	0.7075
D1039-2H	N33°32′30.18″; E80°07′18.35″	Quartz monzonite	1.66	0.710133	0.000005	0.7064
D1039-3H	N33°32′30.18″; E80°07′18.35″	Granite	15.32	0.741999	0.000005	0.7073
D1046H	N33°22′40.19″; E81°34′18.92″	Diorite	0.46	0.709595	0.000006	0.7088
D1048H	N33°22′4.61″; E81°34′4.31″	Porphyritic granodiorite	0.65	0.710304	0.000008	0.7092
D1049H	N33°22′3.96″; E81°34′19.58″	Monzonite	0.65	0.70929	0.000008	0.7082
D1049-2H	N33°22′3.96″; E81°34′19.58″	Granodiorite	0.05	0.70964	0.000006	0.7096
PBN-50-1	N33°22′4.1″; E81°34′19.9″	Porphyritic granodiorite	0.12	0.710182	0.000016	0.7100
PBN-50-2	N33°22′4.1″; E81°34′19.9″	Diorite	0.12	0.710446	0.000014	0.7102
PBN-51-1	N33°22′1.0″; E81°33′52.5″	Porphyritic granodiorite	1.19	0.710644	0.000016	0.7086
BL-1	Bolong, drill core	Porphyritic diorite	0.75	0.706715	0.000015	0.7055

The initial age-corrected ratios $(^{87}Sr/^{86}Sr)_i$ are calculated using the published ages shown in Table 2 and the CHUR isotope ratios ($^{87}Rb/^{86}Sr_{CHUR}$ (t = 0) = 0.0827, $^{87}Sr/^{86}Sr_{CHUR} = 0.7045$). A decay constant λ_{Rb-Sr} of 1.42×10^{-11} a^{-1} is used. $(^{87}Sr/^{86}Sr)_i = (^{87}Sr/^{86}Sr) - ^{87}Rb/^{86}Sr\ (e^{\lambda t} - 1)$.

Table 2
Sm—Nd isotopic compositions of granitoids in ZDMA.

Sample no.	Published U—Pb ages and references	$^{147}Sm/^{144}Nd$	$^{143}Nd/^{144}Nd$	(2σ)	$(^{143}Nd/^{144}Nd)i$	εNd(t)	TDM (Ga)
D1034H	168.3 Ma (Zhang et al., 2011)	0.12	0.512459	0.000005	0.5123	−1.8	1.08
D1034-2H		0.11	0.512409	0.000007	0.5123	−2.7	1.12
D1034-3H		0.13	0.512365	0.000003	0.5122	−3.9	1.44
D1034-4H		0.11	0.512368	0.000004	0.5122	−3.5	1.19
D1035H		0.12	0.512289	0.000005	0.5122	−5.1	1.38
D1035-2H		0.13	0.512302	0.000009	0.5122	−5.0	1.48
PBN-53-3	165.1 Ma (Zhang et al., 2015)	0.14	0.512352	0.000008	0.5122	−4.3	1.58
PBN-53-8		0.12	0.512296	0.000008	0.5122	−5.1	1.43
PBN-54-1		0.10	0.512268	0.000009	0.5122	−5.2	1.19
D1037H	159.96 Ma, 159.40 Ma (Zhang et al., 2011; Li et al., 2014a)	0.13	0.512424	0.000004	0.5123	−2.6	1.25
D1039H		0.09	0.512421	0.000004	0.5123	−2.0	0.89
D1039-2H		0.12	0.512289	0.000007	0.5122	−5.2	1.36
D1039-3H		0.12	0.512281	0.000006	0.5122	−5.4	1.4
D1046H	118.6 Ma (Li et al., 2014a)	0.11	0.512185	0.000003	0.5121	−7.6	1.45
D1048H		0.11	0.512182	0.000003	0.5121	−7.6	1.48
D1049H		0.11	0.512201	0.000004	0.5121	−7.2	1.39
D1049-2H	119.9 Ma (Zhang et al., 2015)	0.14	0.512145	0.000004	0.5120	−8.7	2.04
PBN-50-1		0.16	0.512152	0.000008	0.5120	−9.0	3.03
PBN-50-2		0.16	0.512152	0.000007	0.5120	−8.9	2.63
PBN-51-1		0.11	0.512179	0.000006	0.5121	−7.6	1.42
BL-1	~118 Ma (Chen et al., 2013)	0.11	0.512483	0.000007	0.5124	−1.8	1.02

The initial age-corrected ratios εNd_i are calculated using the published ages and the CHUR isotope ratios ($^{147}Sm/^{144}Nd_{CHUR} = 0.1967$, $^{143}Nd/^{144}Nd_{CHUR} = 0.512638$). A decay constant λ_{Sm-Nd} of 6.54×10^{-12} a^{-1} is used. $(^{143}Nd/^{144}Nd)_i = (^{143}Nd/^{144}Nd) - (^{147}Sm/^{144}Nd) \times (e^{\lambda t} - 1)$. $\varepsilon Nd(t) = [(^{143}Nd/^{144}Nd)_i / (^{143}Nd/^{144}Nd)_{CHUR(t)} - 1] \times 10^4$. $(^{143}Nd/^{144}Nd)_{CHUR(t)} = 0.512638 - 0.1967 \times (e^{\lambda t} - 1)$. $T_{DM} = 1/\lambda \times \ln\{1 + [((^{143}Nd/^{144}Nd) - 0.51315) / ((^{147}Sm/^{144}Nd) - 0.21317)]\}$. $\lambda_{Sm-Nd} = 6.54 \times 10^{-12}$ a^{-1}.

1.5–7.0 wt%). As shown in Fig. 5A and B, the Early Cretaceous Duolong ore-forming porphyry and the Fuye quartz diorite intrusion, which contains a small magnetite deposit, exhibit wide ranges of SiO_2, total alkali, and K_2O contents, on account of late-stage alteration (Zhu et al., 2015b). On an A/NK–A/CNK diagram (Fig. 5C), the samples in the group of normal calc-alkaline and

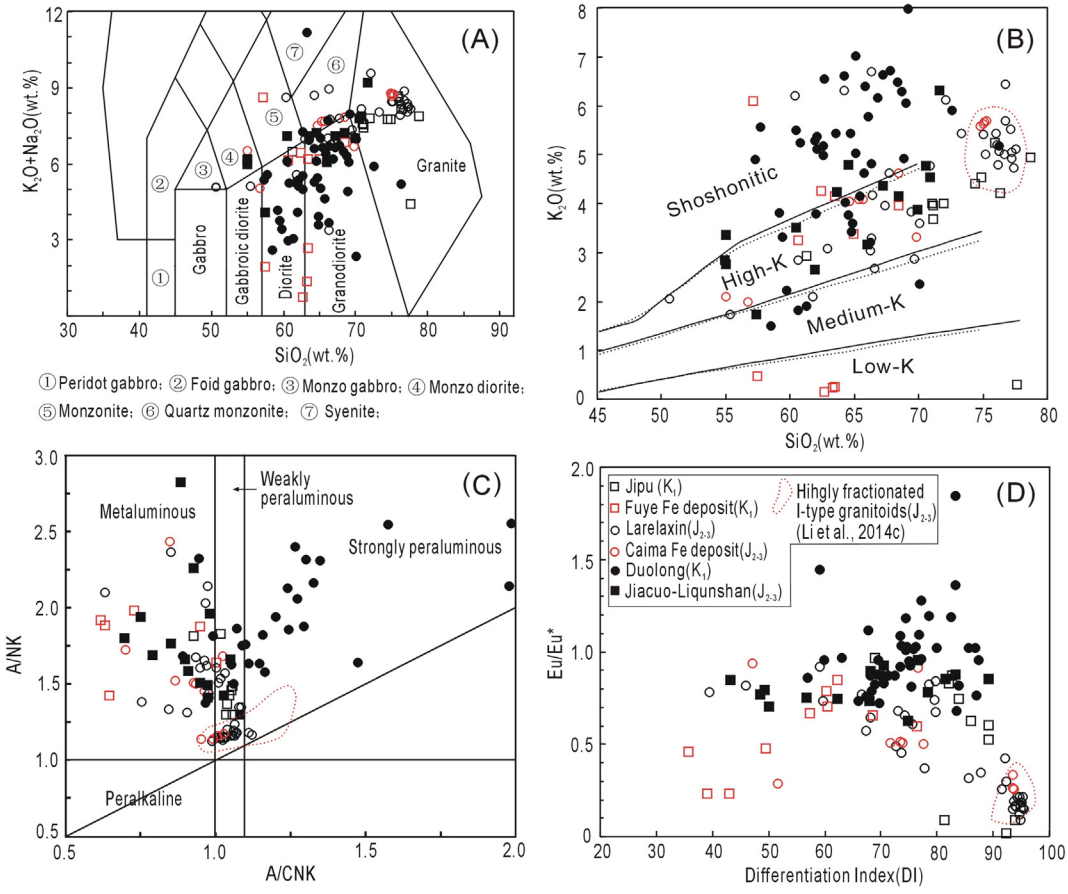

Fig. 5. General classification of granitoids in the ZDMA. (A) $K_2O + Na_2O$ vs. SiO_2 classification diagram from Middlemost (1994). (B) Plot of K_2O vs. SiO_2; most samples belong to the high-K calc-alkaline and shoshonite series. (C) Plot of A/NK vs. A/CNK (Shand, 1943) showing the weakly peraluminous–metaluminous nature of most Middle–Late Jurassic granitoids in the ZDMA, as distinct from the strongly peraluminous nature of the Early Cretaceous Duolong porphyry. (D) Plot of Eu/Eu* vs. Differentiation Index (DI). $Eu/Eu^* = Eu_N / (Sm_N \times Gd_N)^{1/2}$ (N denotes chondrite-normalized values from Sun and McDonough (1989)); DI = Quartz (Qtz) + Orthoclase (Or) + Albite (Ab) + Nepheline (Ne) + Leucite (Lc) + K-feldspar (Kfs), with values calculated according to the CIPW norm. The compositional range of Middle–Late Jurassic highly fractionated I-type granitoids is from Li et al. (2014c).

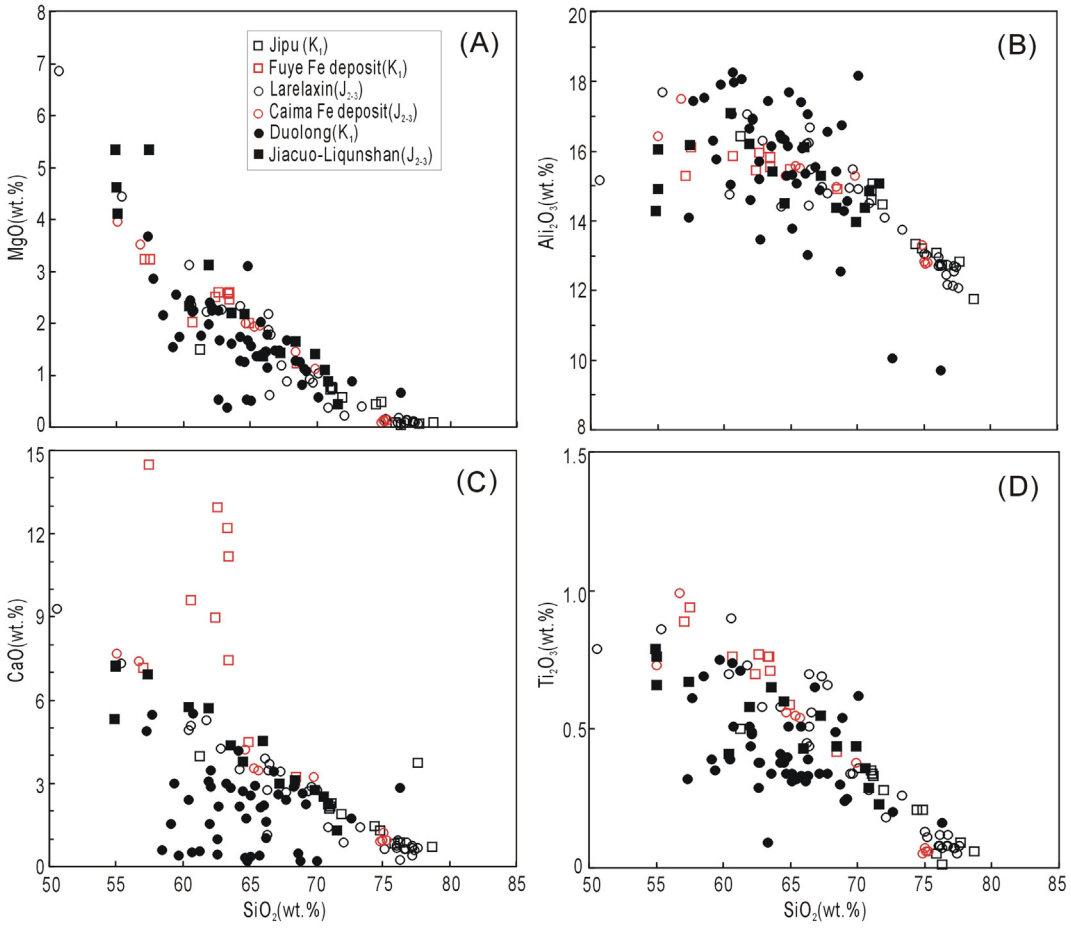

Fig. 6. Harker diagrams of selected major elements showing roughly complete differentiation curves. A small compositional gap occurs at SiO_2 = 73–74 wt%, which separates the highly differentiated granitoids to the right from normal calc-alkaline and shoshonitic granitoids to the left.

shoshonitic I-type granitoids are mostly weakly peraluminous and metaluminous; however, the Duolong porphyries are mostly strongly peraluminous. The differentiation index (DI) values of the samples vary, mainly in the range of 55–82 (Fig. 5D). On major element Harker diagrams, the values of MgO, Al_2O_3, CaO, and TiO_2 typically show negative correlations with SiO_2 and show trends indicating differentiation (Fig. 6). Granitoids of this group are enriched in light rare-earth elements (LREEs) relative to heavy rare-earth elements (HREEs) (LREE/HREE = 3.0–15.0) and large-ion lithophile elements (LILEs) (e.g., Rb, Ba, and Th) as compared with high field-strength elements (HFSEs) (Fig. 7A and B). They exhibit slight or no obvious negative Eu anomalies (Fig. 7A).

(2) Highly fractionated I-type granitoids. In the western part of the ZDMA, the main intrusions (Larelaxin–Caima, J_{2-3}, and Jipu, K_1) are mostly granite and granodiorite (except for mafic dikes and enclaves in the intrusions), with SiO_2 contents mainly in the range of 65–78 wt% (Fig. 5A and B) and high total alkali and K_2O contents ($K_2O + Na_2O$ = 6.0–8.0 wt%; K_2O = 3.0–5.5 wt%). On an A/NK–A/CNK diagram (Fig. 5C), the intrusions are weakly peraluminous and metaluminous. They exhibit relatively high DI values (mainly 70–95) as compared with normal calc-alkaline and shoshonitic granitoids (Fig. 5D). On a Harker diagram, the granitoids show lower contents of MgO, Al_2O_3, CaO, and TiO_2, and higher contents of SiO_2 (Fig 6); they are relatively enriched in LREEs (LREE/HREE = 5.0–17.0) (Fig. 7C) and show typical negative Eu anomalies, but are relatively depleted in P and Ti (Fig. 7D). Their major and trace element geochemistry suggests a high degree of differentiation.

5.2. Whole-rock Rb—Sr and Sm—Nd isotopes

To assess the effects of hydrothermal alteration on the Rb—Sr and Sm—Nd isotopic system, we analyzed the $(^{87}Sr/^{86}Sr)_i$ and εNd(t) values and found no correlation between either value and increasing values of loss on ignition (LOI) (data in Supplementary Table 1). This result suggests that the Sr—Nd isotopic systems have not been affected by alteration (following Yang et al., 2015).

The Middle–Late Jurassic intrusions in the western and eastern segments of the ZDMA show roughly similar Sr—Nd isotope compositions (Fig. 8). The $(^{87}Sr/^{86}Sr)_i$ values of granitoids in Larelaxin–Caima in the western segment are in the range of 0.7029–0.7075, and partly overlap those in Jiacuo–Liqunshan (as represented by the Chaerkangcuo intrusion) in the eastern segment (0.7063–0.7089). The εNd(t) values of −5.39 to −1.76 in the western and −6.30 to −2.10 in the eastern segments show similar ranges. The $T_{(Nd)DM}$ values of 0.89–1.58 Ga in the western and 1.00–1.37 Ga in the eastern segments also show similar ranges (Fig. 8).

The Sr and Nd isotopes of the Early Cretaceous Duolong ore-bearing porphyries are more consistent than those of the Middle–Late Jurassic intrusions (Fig. 8); their $(87Sr/86Sr)_i$ values are in the range of 0.7047–0.7085 and their εNd(t) values are in the range of −8.00 to 4.30 (mainly 0.00 to −4.00). The $T_{(Nd)DM}$ values of the Duolong porphyry are in the range of 0.43–2.15 Ga, but are mostly in the range of 0.90–1.20 Ga (Table 2; Fig. 8). Seven samples of Early Cretaceous metallogenic granitoids from Fuye in the western section of the ZDMA show $(^{87}Sr/^{86}Sr)_i$ values of 0.7082–0.7102 and εNd(t) values of −8.98 to −7.19, with $T_{(Nd)DM}$ values in the range

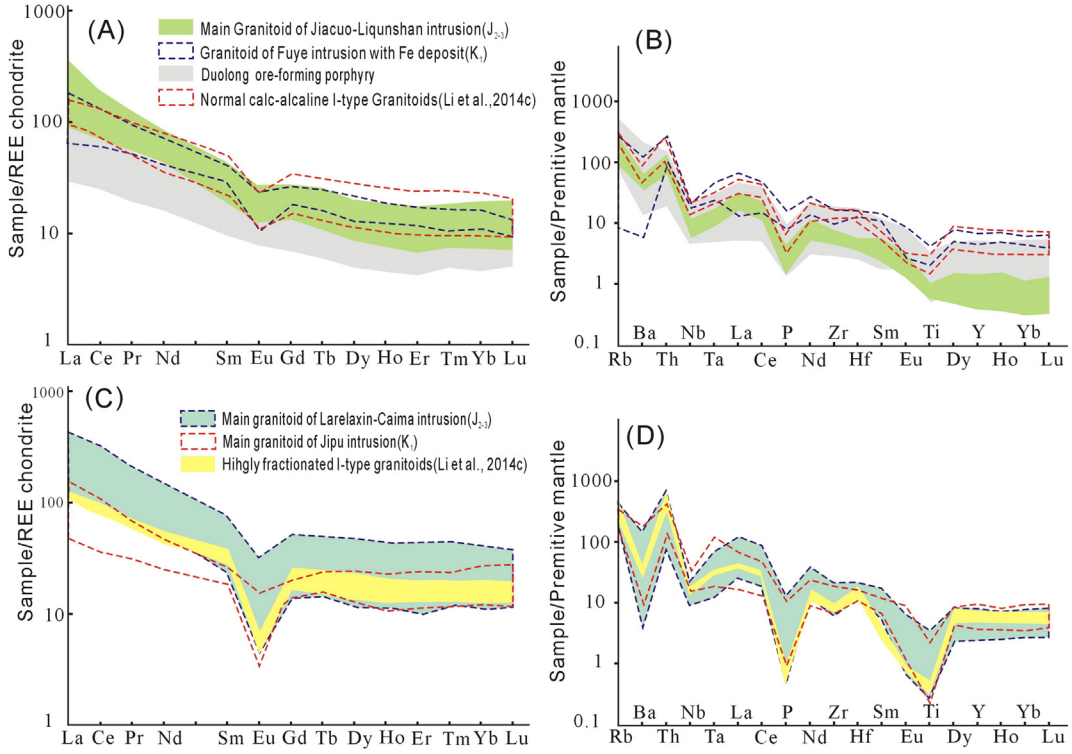

Fig. 7. Chondrite-normalized REE and primitive-mantle-normalized trace element patterns for granitoids in the ZDMA. Normalization data are from Sun and McDonough (1989). (A) and (B) show that most of the granitoid rocks in the ZDMA belong to normal calc-alkaline and shoshonite series. (C) and (D) show data for highly differentiated granitoids.

of 1.39–3.03 Ga, showing large departures from values in the Duolong porphyry. More details of the $(87Sr/86Sr)_i$, εNd(t), and $T_{(Nd)DM}$ data are shown in Fig. 8.

On a $(^{87}Sr/^{86}Sr)_i$–εNd(t) diagram, the Middle–Late Jurassic granite intrusions in the ZDMA roughly overlap those of the Early Cretaceous metallogenic porphyry of the Duolong deposit, but the granitoid of Fuye plots close to Qiangtang basement rocks (Fig. 9). These patterns are consistent with the high $T_{(Nd)DM}$ values of granitoid from Fuye (1.39–3.03 Ga), suggesting a crustal signature for the origin of the Fuye granitoid (Fig. 8).

Ratio	Age	West segment(Zapug-Fuye)		East segment(Duobuza-Liqunshan)	
		Data range and average value	Intrusion	Data range and average value	Intrusion
$(^{87}Sr/^{86}Sr)_i$	J_{2-3}	0.7029 0.7063 0.7075	Larelaxin-Caima	0.7063 0.7072 0.7089	Jiacuo-Liqunshan
	K_1	0.7082 0.7102 0.7092	Fuye	0.7047 0.7066 0.7085	Duolong
εNd(t)	J_{2-3}	-5.39 -3.98 -1.76	Larelaxin-Caima	-6.30 -4.63 -2.10	Jiacuo-Liqunshan
	K_1	-8.98 -8.08 -7.19	Fuye	-8.00 -2.58 4.30	Duolong
$T_{(Nd)DM}$(Ga)	J_{2-3}	0.89 1.29 1.58	Larelaxin-Caima	1.00 1.23 1.37	Jiacuo-Liqunshan
	K_1	1.39 1.92 3.03	Fuye	0.43 1.12 2.15	Duolong
εHf(t)	J_{2-3}	-19.4 -3.9 9.7	Larelaxin	-18.6 -4.4 2.5	Jiacuo-Liqunshan
		-5.8 -1.9 2.3	Caima		
	K_1	-13.0 -9.8 -5.2	Fuye	-10.7 -8.0 6.4	Jiacuo-Liqunshan
		-13.0 -8.6 -1.9	Jipu	-13.0 5.9 12.0	Duolong
				-13.0 -1.7 4.0	Qingcaoshan-Xianqian

Fig. 8. Summary of whole-rock Sr—Nd and zircon Hf isotopic data for rocks in the ZDMA, showing $(^{87}Sr/^{86}Sr)_i$, εNd(t), and εHf(t) values of Middle–Late Jurassic to Early Cretaceous granitoids in the western and eastern segments of the ZDMA.

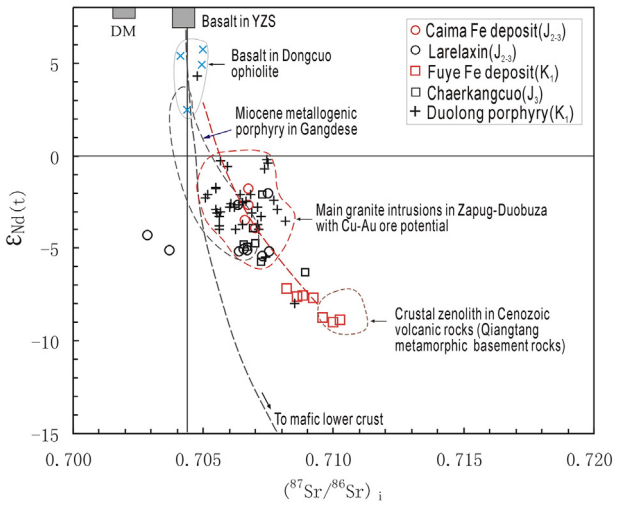

Fig. 9. A $(^{87}Sr/^{86}Sr)_i$–εNd(t) diagram showing data for granite intrusions in the Zapug–Duobuza zone. The data for depleted mantle (DM), mafic lower crust, basalt in the Yarlung Zangbo suture (YZS), and Miocene metallogenic porphyry in the Gangdese are from Miller et al. (1999); Hou et al. (2011); Hu et al. (2012), and Yang et al. (2015). Data for crustal xenoliths in Cenozoic volcanic rocks are from Lai and Qin (2008) and Li et al. (2014b). Data for basalt in the Dongcuo ophiolite are from Bao et al. (2007).

6. Ore-forming potential of major granite intrusions in the ZDMA

Geochemical studies suggest that both mantle and crustal sources contributed to the formation of Cu, Fe, and Pb—Zn deposits in the ZDMA and the Gangdese zone, despite that the two zones exist in different tectonic settings (accretionary orogen and continental collision, respectively) (Hou and Zhang, 2015; Li et al., 2014a; Richards, 2015; Yang et al., 2015). Thus, a comparison of whole-rock Sr—Nd and zircon Hf isotopic compositions of granitoids in the ZDMA with some major deposits in the Gangdese zone would be helpful for revealing their ore-forming potential.

6.1. Zircon Hf isotopic data

Published zircon Hf isotopic data for most of the granitic intrusions in the ZDMA have enabled a systematic analysis of their magma sources and ore-forming potential. The zircon εHf(t) values are summarized and displayed graphically in Fig. 8, and Fig.10 shows a plot of zircon εHf(t) values against age. The εHf(t) values for several giant porphyry Cu deposits in the ZDMA and Gangdese belts, including the Duolong, Qulong (10 Mt Cu) and Jiama (6 Mt Cu) deposits, are mostly positive (2 − 11), indicating that the magmas were derived mainly from mantle sources. On the other hand, the Pb—Zn-bearing granitoids exhibit negative εHf(t) values (− 19.0 to − 2.5), as displayed by the Yaguila Pb—Zn deposit (Fig. 10).

The Middle–Late Jurassic intrusions in the western and eastern segments of the ZDMA exhibit similar εHf(t) values to each other, as shown by the intrusions in the Larelaxin (− 19.4 to 9.7), Caima (− 5.8 to 2.3), and Jiacuo–Liqunshan (− 18.6 to 2.5) districts (Figs. 8 and 10). These results suggest the involvement of both mantle and crustal materials in the magma resources. Although the εHf(t) values as a whole are lower than those of the Cu-bearing porphyries in Duolong (mainly 2.0 to 11.5), Qulong–Jiama (mainly 2.6 to 12.0), and other super-large Cu deposits, the values of the main granites in both the Jiacuo–Liqunshan and Larelaxin–Caima districts overlap with those of the Qingcaoshan–Xianqian Cu deposits (− 13.0 to 4.0) in the north of Duolong, and the Chengba (− 1.0 to 4.0) and Sharang (− 2.5 to 2.0) porphyry Cu—Mo deposits in the Gangdese (Fig. 10). Therefore, the Middle–Late Jurassic granite intrusions may have the

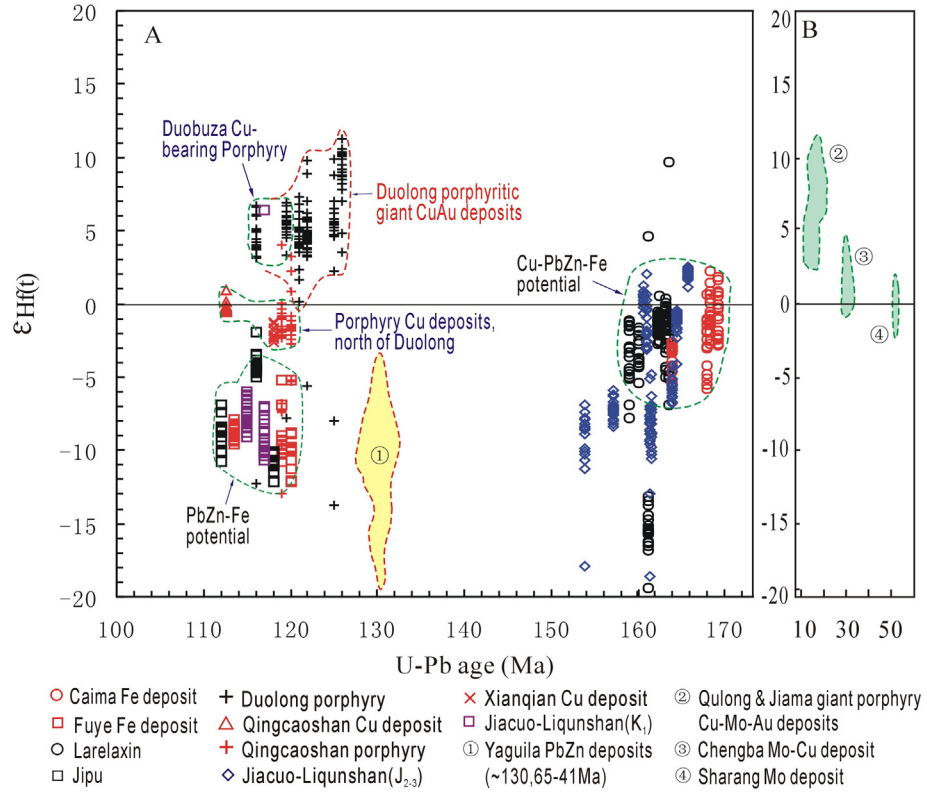

Fig. 10. (A) Zircon εHf(t) values plotted against the age of granitoids in the ZDMA and Yaguila in the central Gangdese zone. (B) Zircon εHf(t) values plotted against the age of ore-forming porphyries in the Gangdese zone. The zircon Hf isotope data for granitoids in the ZDMA are from Chen et al. (2013); Li et al. (2014a,b), and Zhang et al. (2015). Data for the granitoids from the Yaguila Pb—Zn deposit, the Sharang Mo deposit in the central Gangdese, and the Qulong, Jiama, and Chengba porphyritic Cu—Mo—Au deposits in the south Gangdese are from Yang et al. (2009); Hou et al. (2011), and Wang et al. (2012), respectively.

potential for Cu—Fe—Pb—Zn polymetallic deposits, as suggested by the combined mantle and crustal (or heterogeneous source) contributions to their magmas.

Early Cretaceous granitoids in the ZDMA exhibit a wide range of εHf(t) values, from negative to positive (Figs. 8 and 10), and their characteristics can be summarized as follows. (1) Similarly to Miocene Cu-bearing porphyries in the south Gangdese, the Duolong Cu-bearing porphyries exhibit relatively high εHf(t) values (mainly 2.0 to 11.5), indicating an enhanced contribution of mantle-derived components to the Cu and Au deposits. (2) The porphyritic granitoids of Qingcaoshan and Xianqian exhibit εHf(t) values of −13.0 to 4.0. (3) Granitoids with negative εHf(t) values, including at Fuye (−13.0 to −5.2) and Jipu (−13.0 to −1.9) in the western segment and Jiacuo–Liqunshan (mainly −10.7 to −6.0) in the eastern segment, are indicative of a crustal origin.

6.2. Comprehensive analysis of the ore-forming potential of major granite intrusions in the ZDMA

Whole-rock Sr—Nd and zircon Hf isotopic signatures reveal similar information regarding the ore-forming potential of major granite intrusions. The Early Cretaceous Duolong porphyry and the Middle–Late Jurassic granitoids in the ZDMA partially overlap with the Miocene Cu-bearing porphyry in Gangdese (Fig. 9), suggesting a much greater contribution of basalt to their magmas than to the Early Cretaceous Fuye Fe-bearing granite intrusion. The Fuye intrusion originated mainly from the lower crust of the Qiangtang terrane (Fig. 9).

Lithogeochemical and comparative studies suggest that source rock components, host rock lithologies, and tectonic setting are major factors contributing to the metallogenetic potential of granitoids (Table 3). Greater contributions of mantle-derived components in granitic magma and fore-arc accretionary turbidite host rocks benefit the formation and preservation of porphyry Cu—Au deposits, thus indicating the ore-forming potential of the Qingcaoshan–Xianqian region to the north of Duolong, located in the eastern prospecting district (Li et al., 2013; Hou et al., 2015). A comprehensive study has shown that Middle–Late Jurassic granite intrusions in the regions of Larelaxin–Caima and Jiacuo–Liqunshan exhibit characteristics favorable for skarn-type and hydrothermal metallogenesis, thus indicating two new potential prospecting districts for Cu—Au, Fe, and Pb—Zn deposits (Table 3).

7. Discussion of the regional tectonic evolution

7.1. Triassic folding of Permo-Carboniferous rocks surrounding the ZDMA

The presence of glutenite at the base of upper Triassic strata, unconformably overlying formations in the south Qiangtang and Longmucuo–Shuanghu zones, represents the occurrence of a Triassic orogenic event (Roger et al., 2008). The upper Triassic Tumengela Formation. (T_3t) is composed of clastic sedimentary rocks with coal interbeds and plant and bivalve fossils, representing a marine–subaerial transitional facies and indicating the closure of the Longmucuo–Shuanghu paleo-Tethys Ocean and related orogenesis (Zhao et al., 2001; Wang et al., 2004; Li et al., 2007). However, the uplift zone is exposed only in the eastern part of the Qiangtang terrane, where it is referred to as the Tumengela uplift. The upper Triassic unconformity does not occur throughout the south Qiangtang terrane, although orogenesis resulted in the widespread folding of Permo-Carboniferous strata, which were later intruded by Middle Jurassic–Early Cretaceous granites, resulting in the formation of skarn-type ores in the west prospecting district in the ZDMA (Fig. 3).

7.2. Jurassic Tethys evolution of the BNS

The Tethys ocean basin, formerly located in the middle and western sections of the BNS, experienced extension and expansion during the Middle–Late Triassic, at which time the Quehala Group ($T_{2-3}Q$) sediments were deposited. The Quehala Group comprises glutenite, quartz sandstone, siltstone, and black slate, indicating passive-margin rifting, extension, and basin-deepening (Zhu et al., 2011a,b). An Early Jurassic deep ocean basin formed between the Lhasa and south Qiangtang terranes (Fig. 11A); however, stratigraphic data suggest that this deep basin existed only during the Early Jurassic, as verified by flysch sediments of the lower Mugagangri Group ($J_{1-2}M$) (Geng et al., 2011, 2013). The basin experienced subduction of oceanic crust and narrowing in the Middle Jurassic, when it became a shallow-sea basin (Wang et al., 2008; Li et al., 2014a; Zhu et al., 2015a). The northward subduction led to the formation of a magmatic arc (as represented by Middle Jurassic granites in the ZDMA) and resulted in the formation of a residual sea basin during the Late Jurassic–Early Cretaceous (Li et al., 2014c; Zhu et al., 2015a). The Middle Jurassic shallow-sea clastic sediments containing coral, polyp, and sporopollen fossils in the Nyima and Rebuka areas are conformably overlain by Late Jurassic beach-facies carbonate sediments of the Shamuluo Fm. (Ji et al., 2011). Fossils found to the north of Wuma in Gerze County suggest that the Late Jurassic strata in the BNS are mainly successive carbonate sediments (Ji et al., 2011). A series of fluvial–littoral-facies clastic rocks containing Early Cretaceous foraminifera (*Mesorbitolina* sp.) and plant fossils crops out in the Gase area, Nyima County (Ji et al., 2011). Recent geological surveys in the middle and western sections of the BNS suggest that deep-ocean flysch deposits occur in the lower part of the Mugagangri Group ($J_{1-2}M$), whereas the upper part is composed of tectonic mélange (Geng et al., 2015). These lines of evidence suggest that the Early Jurassic deep ocean basin evolved into a residual marine basin in Late Jurassic–Early Cretaceous times (Fig. 11B).

7.3. Flat subduction model

The flat subduction and slab break-off model proposed for the Andes continental arc explains the generation of intensive arc magmatism and numerous large porphyry Cu deposits (Schütte et al., 2010; Cao et al., 2011; Bissig et al., 2014). Cao et al. (2011) first raised the possibility of northward flat subduction and related porphyry Cu deposits in the regions of Gerze and Duolong. According to this model, early-stage northward flat subduction occurred in the region at ca. 170–150 Ma, and

Table 3
Summary of the ore-forming potentials of major granitic intrusions in the ZDMA.

	Western segment			Eastern segment		
Intrusions	Larelaxin–Caima	Jipu	Fuye	Jiacuo–Liqunshan	Duolong	Qingcaoshan–Xianqian
Ages of granitoids	J_{2-3}	K_1	K_1	J_{2-3}	K_1	K_1
Host rock	Permo-Carboniferous and Triassic carbonate and clastic sedimentary rocks, representing stable basins on the northern passive margin of Gondwanaland.				Jurassic turbidite series in fore-arc accretionary mélanges, representing juvenile crust.	
Major and trace element signature	Highly fractionated I-type granitoids			Normal calc-alkaline and shoshonitic I-type granitoids		
Source rock signature	Both mantle and crustal materials	Crustal origination		Both mantle and crustal materials	Enhanced mantle contributions	Both mantle and crustal materials
Ore-forming potential	Skarn and hydrothermal polymetal	Weak Fe	Weak Fe, Pb, Zn	Skarn and hydrothermal polymetal	High potential for porphyry Cu—Au deposits	

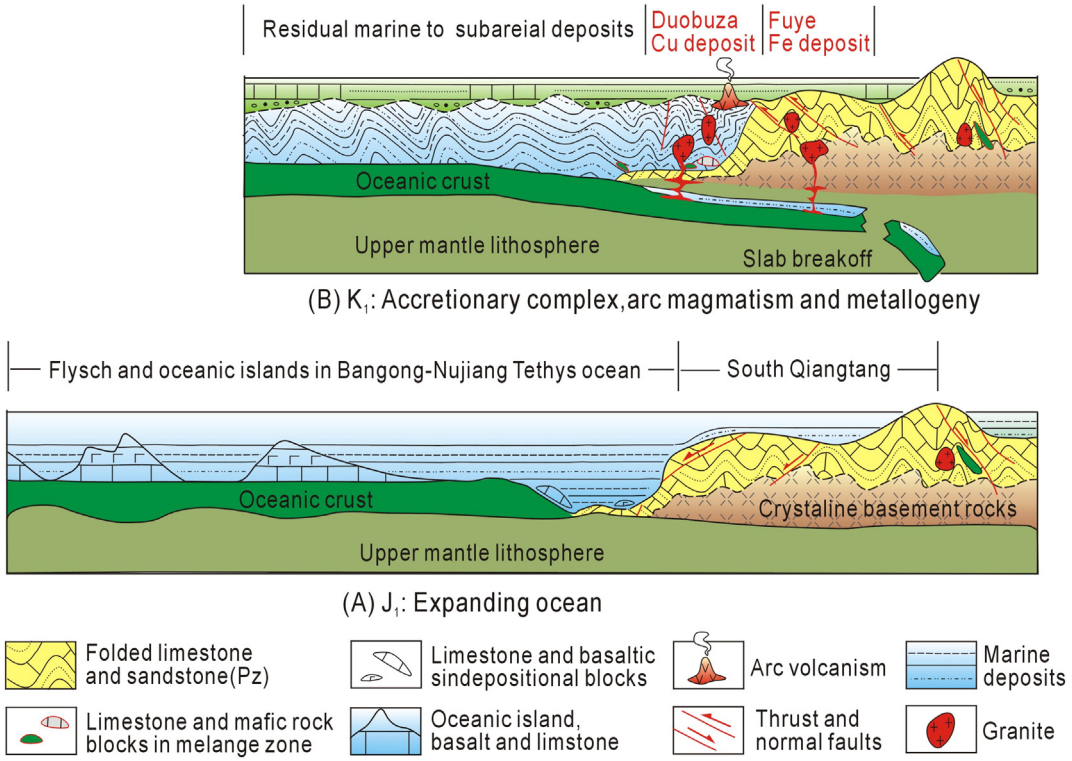

Fig. 11. Tethyan evolution in the western BNS, and related metallogenesis during the Early Jurassic–Early Cretaceous.

break-off of the subducting slab accompanied peak arc magmatism and metallogenesis at ca. 125–110 Ma (Fig. 11). These processes are supported by the following six lines of evidence.

(1) Anomalously thick oceanic crust. Many ophiolite outcrops occur in Dongcuo and Nadong, Gerze County, and tectonic remnants of massive oceanic islands are distributed within the BNS in this area. These remnants are composed of alternating beds of limestone and basalt, >1000 m thick (Tibet Institute of Geological Survey, 2012; Fan et al., 2014a,b). The Dongcuo residual ophiolite block is >6 km thick (Bao et al., 2007). The short-lived small, deep Bangong Co–Nujiang ocean basin was filled by a sequence of terrigenous clastic rocks >3000 m thick, represented by the Mugagangri Group ($J_{1-2}M$); these sediments were deposited on mafic oceanic crust (Wang et al., 2008; Qu et al., 2013). It can therefore be concluded that the low-density thickened oceanic subducting slab was probably >10 km thick. This anomalously thick oceanic crust contained massive clastic rocks, oceanic islands, and seamounts, and was more buoyant than normal oceanic crust, thus favoring the occurrence of low-angle flat subduction (Ramos and McNulty, 2002; Martinod et al., 2010; Cao et al., 2011).

(2) Sr—Nd isotopic evidence. Two lines of Sr—Nd isotopic evidence suggest that two magma components were involved in the two-stage granitic magmatism: a variable sialic crust component and subducted basaltic crust with an OIB (Ocean Island Basalt) geochemical signature. (a) A $(^{87}Sr/^{86}Sr)_i$–εNd(t) diagram shows that both the Early Cretaceous Duolong porphyry and the Middle–Late Jurassic granite intrusions in the ZDMA lie on a mixing curve between Dongcuo basalt and Qiangtang metamorphic basement rocks, with the two end-members representing the source rocks of the two-stage granite intrusions (Fig. 9). (b) According to Lai and Qin (2008), the crust located 30 km below the Qiangtang terrane is not composed of mafic rocks, as generally documented, but is metamorphic basement consisting of mostly ancient sedimentary rocks. For example, basalt in the Dongcuo ophiolite block in the BNS is a basanitoid that is not a typical MORB, but is rather an oceanic island basalt, formed from enriched mantle (EM I) (Bao et al., 2007).

(3) An anomalously wide magmatic arc belt. As stated above, Middle Jurassic–Early Cretaceous granites and volcanic rocks are sporadically exposed in N–S-trending outcrops in a belt more than 200 km wide, in the western part of the south Qiangtang terrane, to the north of the BNS. The south Qiangtang terrane experienced folding and southward thrusting, resulting in terrain shortening of >150 km (Kapp et al., 2005). Arc magma tended to migrate from the interior of the south Qiangtang terrane southward to Liqunshan, Jiacuo, and Duobuza areas, as shown in Fig. 1B. Therefore, the presence of an anomalously wide zone of arc magmatism agrees with the occurrence of long-distance flat subduction. Ophiolite remnants are present in the Chaerkangcuo area in the south Qiangtang terrane, far from the BNS, a location that was likely the result of flat subduction (Fig. 1B).

(4) A magmatic quiet period. The subducted slab gradually cooled because of long-distance flat subduction, and the slab temperature decreased to less than the minimum temperature of partial melting, leading to a magmatic quiet period. Flat subduction zones in the Andes and South America show a magmatic quiet period in the Quaternary (Murphy et al., 2003; Cao et al., 2011). An approximately 10-Myr period of intermittent arc magmatism occurred during 140–130 Ma in the ZDMA in the south Qiangtang terrane (Fig. 4), indicating that northward flat subduction of the BNS Tethys oceanic crust had entered a late stage of evolution.

(5) Sr—Nd and Hf isotopic evidence. The whole-rock Sr—Nd and zircon Hf isotope compositions of Early Cretaceous granites are very different from those of Middle–Late Jurassic granites (Fig. 8), and can be interpreted in terms of a transformation in tectonic setting. The magma sources of Early Cretaceous granites changed after the magmatic quiet period, during 130–110 Ma.

(6) Early Cretaceous peak magmatism and slab break-off. The period of Early Cretaceous peak magmatism was associated with the formation of porphyry Cu deposits. It can be inferred that the flat

subducting slab broke off in the Early Cretaceous, followed by asthenospheric upwelling, which produced enormous amounts of heat and caused partial melting of the subducted slab and lower Qiangtang crust. Peak magmatism occurred at 125–110 Ma. Qu et al. (2013) reported an A-type granite in the BNS with an age of ca. 110 Ma, and Chang et al. (2011) reported the Early Cretaceous Rena–Co rhyolites in south Qiangtang (Fig. 1B). Both can be interpreted as results of slab break-off in the Early Cretaceous. On the other hand, the existence of ~116 Ma oceanic islands in the BNS suggests that the BNS was still a residual marine basin in the Early Cretaceous (Fan et al., 2014a,b). Final closure of the marine basin and a collisional orogeny is indicated by the existence of Late Cretaceous red beds in the south Qiangtang and north Lhasa terranes (Geng et al., 2011; Zhu et al., 2015a).

Although the above evidence may support a flat subduction model within the ~400-km-long ZDMA and western BNS, no similar magmatic arc is exposed in the eastern part of the south Qiangtang terrane, which is >1000 km long and trends east–west. Therefore, the northward subduction model of the BNS Tethys Ocean crust and related arc magmatism requires further constraints to more fully understand the tectonic evolution of the area.

8. Conclusions

(1) The ZDMA is composed of small scattered granite (porphyry) intrusions and minor volcanic rocks that formed in two magmatic stages, at 170–150 Ma and 130–110 Ma. Late Cretaceous to Paleogene thrusting in the south Qiangtang terrane could have buried part of the ZDMA.

(2) The widely distributed Middle–Late Jurassic granite intrusions in the ZDMA exhibit Sr—Nd isotopic characteristics similar to those of ore-bearing porphyries in the Duolong giant Cu—Au deposits. Although the εHf(t) values of most granites in the Jiacuo–Liqunshan and Larelaxin–Caima districts are generally lower than those of the Cu-bearing porphyries in the Duolong and Gangdese zones, they overlap with those of the Qingcaoshan and Xianqian Cu deposits in the north of Duolong and the Chengba and Sharang porphyry Cu—Mo deposits in the Gangdese. The Sr—Nd—Hf isotopic data suggest variable contributions of mantle-derived material and Qiangtang crustal sources of granites, and indicate two new potential prospecting districts with potentials for Cu—Au, Fe, and Pb—Zn ores, in the Jiacuo–Liqunshan and Larelaxin–Caima areas.

(3) Except for the Duolong ore-forming porphyries, which show enhanced mantle contributions and intruded an accretionary mélange, the Early Cretaceous granites in other areas in this belt are mostly of crustal origin, derived from source rocks consisting of Qiangtang felsic basement and Permo-Carboniferous strata. These observations indicate the low ore-forming potential of skarn-type Fe and Pb—Zn deposits.

(4) The western BNS was the location of a short-lived deep-ocean basin in the Early Jurassic. The region possibly experienced northward flat subduction during the Middle–Late Jurassic, with a period of intermittent magmatism during the late stage of flat subduction at 140–130 Ma. The break-off of subducted slab and partial melting of both subducted slab with an OIB signature and the lower Qiangtang crust caused peak arc magmatism and intensive metallogenesis at 125–110 Ma. However, the flat subduction model requires further constraints to more fully understand the tectonic history of the area.

Supplementary data to this article can be found online at http://dx.doi.org/10.1016/j.oregeorev.2016.02.018.

Acknowledgments

This research was supported by the Natural Science Foundation of China (grants 41273047, 41303043, 41402058, and 41202049) and a CGS project (12120113036500). The participants of the geological and mineral survey of the Bangong Co–Nujiang metallogenic belt (2010–2015) include the Geological Survey Institute of Jiangxi Province, the Regional Geological Survey Institute of Hebei Province, the Geological Survey Institute of Tibet, Jilin University, China University of Geosciences (Wuhan and Beijing), the Geological Survey Institute of Jilin Province, and other institutions (more than 50 project teams in total). We sincerely thank all of the personnel participating in the geological and mineral survey of the Bangong Co–Nujiang metallogenic belt and also thank Prof. Guitang Pan for his consulting. We thank Prof. Di-Cheng Zhu and Dr. Zhi-Ming Yang for their constructive suggestions that improved the quality of this manuscript.

References

Bao, P.S., Xiao, X.C., Su, L., Wang, J., 2007. Geochemical characteristics and isotopic dating for the Dongco ophiolite, Tibet plateau. Sci. China Ser. D 50 (5), 660–671.
Bissig, T., Figueroa, L.C.M., Hart, C.J.R., 2014. Petrochemistry of igneous rocks of the California-Vetas mining district, Santander, Colombia: implications for northern Andean tectonics and porphyry Cu (–Mo, Au) metallogeny. Lithos 200–201, 355–367.
Cao, M.J., Qin, K.Z., Li, J.L., 2011. Research progress on the flat subduction and its metallogenic effect,two cases analysis and some prospects. Acta Petrol. Sin. 27 (12), 3727–3748 (in Chinese with English abstract).
Chang, Q.S., Zhu, D.C., Zhao, Z.D., Dong, G.C., Mo, X.X., Liu, Y.S., Hu, Z.C., 2011. Zircon U–Pb geochonology and Hf isotopes of the Early Cretaceous Rena-Co rhyolites from southern margin of Qiangtang, Tibet,and their implications. Acta Petrol. Sin. 27 (7), 2034–2044 (in Chinese with English abstract).
Chen, H.A., Zhu, X.P., Ma, D.F., Huang, H.X., Li, G.M., Li, Y.B., Li, Y.C., Wei, L.J., Liu, C.Q., 2013. Geochronology and geochemistry of the Bolong porphyry Cu–Au deposit, Tibet and its mineralizing significance. Acta Geol. Sin. 87 (10), 1–19 (in Chinese with English abstract).
Fan, J.J., Li, C., Xu, J.X., Wang, M., 2014a. Petrology, geochemistry, and geological significance of the Nadong ocean island, Banggongco–Nujiang suture, Tibetan plateau. Int. Geol. Rev. 56 (8), 915–928.
Fan, J.J., Li, C., Xie, C.M., Wang, M., 2014b. Petrology, geochemistry, and geochronology of the Zhonggang ocean island, northern Tibet: implications for the evolution of the Banggongco–Nujiang oceanic arm of the Neo-Tethys. Int. Geol. Rev. 56 (12), 1504–1520.
Geng, Q.R., Sun, Z.M., Pan, G.T., Zhu, D.C., Wang, L.Q., 2009. Origin of the Gangdise (Transhimalaya) Permian arc in southern Tibet: stratigraphic and volcanic geochemical constraints. Island Arc 18, 467–487.
Geng, Q.R., Pan, G.T., Wang, L.Q., Peng, Z.M., Zhang, Z., 2011. Tethyan evolution and metallogenetic geological background of the Bangong Co-Nujiang belt and the Qiangtang massif in Tibet. Geol. Bull. China 30 (8), 1261–1274 (in Chinese with English abstract).
Geng, Q.R., Peng, Z.M., Zhang, Z., Pan, G.T., Wang, L.Q., Guan, J.L., 2012a. Tethyan evolution and geological background of the Bangong Co-Nujiang metallogenetic zone and adjacent region. Geological Publishing House, pp. 1–187 (in Chinese).
Geng Q.R., Peng Z.M., Zhang Z., Pan G.T., Wang L.Q., Guan J.L., 2012b. Geological map of the Bangong Co-Nujiang metallogenetic zone and adjacent region (1:750,000) with a synopsis. Geological Publishing House(in Chinese).
Geng, Q.R., Peng, Z.M., Zhang, Z., Guan, J.L., 2013. Metallogenesis related to magmatic arcs in North and South Sides of the Bangong-Nujiang Suture in Central Tibet. Acta Geol. Sin. (Engl. Ed.) 87 (supp.), 22–24.
Geng, Q.R., Mao, X.C., Zhang, Z., Peng, Z.M., Guan, J.L., 2015. New recognition of magmatic arcs in middle and west part of Bangong-Nujiang metallogenic belt and its guidance on mineral prospecting. Geol. Surv. China 2 (2), 1–11 (in Chinese with English abstract).
Hou, Z.Q., Zhang, H.R., 2015. Geodynamics and metallogeny of the eastern Tethyan metallogenic domain. Ore Geol. Rev. 70, 346–384.
Hou, Z.Q., Zhang, H.R., Pan, X.F., Yang, Z.M., 2011. Porphyry Cu (–Mo–Au) deposits related to melting of thickened mafic lower crust: examples from the eastern Tethyan metallogenic domain. Ore Geol. Rev. 39 (2011), 21–45.
Hou, Z.Q., Duan, L.F., Lu, Y.J., Zheng, Y.C., Zhu, D.C., Yang, Z.M., Yang, Z.S., Wang, B.D., Pei, Y.R., Zhao, Z.D., McCuaig, T.C., 2015. Lithospheric architecture of the Lhasa Terrane and its control on Ore deposits in the Himalayan-Tibetan Orogen. Econ. Geol. 110, 1541–1575.
Hu, Y.B., Liu, J.Q., Ling, M.X., Ding, W., Liu, Y., Zartman, R.E., 2012. The formation of Qulong adakites and their relationship with porphyry copper deposit: geochemical constraints. Lithos 220-223, 60–80.
Ji, Z.S., Yao, J.X., Wu, G.C., 2011. Discovery of the Late Jurassic coral fauna in the Tukari Formation at northern Oma Village, Gêrzê County, Tibet, China and its geological significances. Geol. Bull. China 30 (2/3), 418–438 (2011, in Chinese with English abstract).
Kapp, P., Murphy, M.A., Yin, A., Harrison, T.M., Ding, L., Guo, J., 2003a. Mesozoic and Cenozoic tectonic evolution of the Shiquanhe area of western Tibet. Tectonics 22 (4), 1029. http://dx.doi.org/10.1029/2001TC001332 (4).
Kapp, P., Yin, A., Manning, C.E., Harrison, T.M., Taylor, M.H., 2003b. Tectonic evolution of the early Mesozoic blueschist-bearing Qiangtang metamorp belt, central Tibet. Tectonics 22 (4), 1043–1069.

Kapp, P., Yin, A., Harrison, T.M., Ding, L., 2005. Cretaceous-Tertiary shortening, basin development, and volcanism in central Tibet. GSA Bull. 117 (7–8), 865–878.
Lai, S.C., Qin, J.F., 2008. Petrology and geochemistry of the granulite xenoliths from Cenozoic Qiangtang volcanic field: implication for the nature of the lower crust in the northern Tibetan plateau and the genesis of Cenozoic volcanic rocks. Acta Petrol. Sin. 24 (2), 325–336 (in Chinese with English abstract).
Leloup, P.H., Arnaud, N.O., Mahéo, G., Paquette, J.L., Guillot, S., Valli, F., Li, H., Xu, Z., Lacassin, R., Tapponnier, P., 2012. Successive deformation episodes along the Lungmu Co zone, west-central Tibet. Gondwana Res. 21, 37–52.
Li, C., Zhai, Q.G., Dong, Y.S., Yu, J.J., Huang, X.P., 2007. Establishment of the upper Triassic Wanghuling Formation at Guoganjianian Mountain, central Qiangtang, Qinghai-Tibet Plateau, and its significance. Geol. Bull. China 26 (8), 1003–1008 (in Chinese with English abstract).
Li, G.M., Duan, Z.M., Liu, B., Zhang, H., Dong, S.L., Zhang, L., 2011a. The discovery of Jurassic accretionary complexes in Duolong area, northern Bangong Co-Nujiang suture zone, Tibet, nd its geologic significance. Geol. Bull. China 30 (8), 1256–1260 (in Chinese with English abstract).
Li, G.M., Li, J.X., Qin, K.Z., Duo, J., Zhang, T.P., Xiao, B., Zhao, J.X., 2011b. Geology and hydrothermal alteration of the Duobuza Gold-Rich Porphyry Copper District in the Bangongco Metallogenetic Belt, Northwestern Tibet. Resour. Geol. 62 (1), 99–118.
Li, Y.B., Duo, J., Zhong, W.T., Li, Y.C., Qiang, B., Wang, D., Chen, H.Q., 2012. An exploration model of the Duobuza porphyry Cu–Au deposit in Gaize Country, northern Tibet. Geol. Explor. 48 (2), 274–287 (in Chinese with English abstract).
Li, J.X., Qin, K.Z., Li, G.M., Xiao, B., Zhao, J.X., Cao, M.J., Chen, L., 2013. Petrogenesis of ore-bearing porphyries from the Duolong porphyry Cu–Au deposit, central Tibet: evidence from U–Pb geochronology, petrochemistry and Sr–Nd–Hf–Oisotope characteristics. Lithos 160–161 (2013), 216–227.
Li, J.X., Qin, K.Z., Li, G.M., Jeremy, P.R., Zhao, J.X., Cao, M.J., 2014a. Geochronology, geochemistry, and zircon Hf isotopic compositions of Mesozoic intermediate–felsic intrusions in central Tibet: petrogenetic and tectonic implications. Lithos 198–199, 77–91.
Li, J.X., Qin, K.Z., Li, G.M., Xiao, B., Zhao, J.X., Chen, L., 2014b. Petrogenesis of Cretaceous igneous rocks from the Duolong porphyry Cu–Au deposit, central Tibet: evidence from zircon U–Pb geochronology, petrochemistry and Sr–Nd–Pb–Hf isotope characteristics. Geol. J. http://dx.doi.org/10.1002/gj.2631 (Published online in Wiley Online Library (wileyonlinelibrary.com)).
Li, S.M., Zhu, D.C., Wang, Q., Zhao, Z.D., Sui, Q.L., Liu, S.A., Liu, D., Mo, X.X., 2014c. Northward subduction of Bangong–Nujiang Tethys: insight from Late Jurassic intrusive rocks from Bangong Tso in western Tibet. Lithos 205 (2014), 284–297.
Li, G.M., Qin, K.Z., Li, J.X., Evans, N.J., Zhao, J.X., Cao, M.J., Zhang, X.N., 2015. Cretaceous magmatism and metallogeny in the Bangong–Nujiang metallogenic belt, central Tibet: evidence from petrogeochemistry, zircon U–Pb ages, and Hf–O isotopic compositions. Gondwana Res. http://dx.doi.org/10.1016/j.gr.2015.09.006.
Liang, X.R., Wei, G.J., Li, X.H., Liu, Y., 2003. Precise measurement of 143Nd/144Nd and Sm/Nd ratios using multiple-collectors inductively coupled plasma-mass spectrometer (MC-ICPMS). Geochimica 32 (1), 91–96 (in Chinese with English abstract).
Liu, Q.H., Xiao, Z.J., Cao, S.H., Liao, L.G., Xiao, Y.B., 2004. A preliminary study of the spatio-temporal framework of the archipelagic arc-basin systems in the western part of the Bangong-Nujiang suture zone, Xizang. Sediment. Geol. Tethyan Geol. 24 (3), 15–21 (in Chinese with English abstract).
Liu, D.L., Shi, R.D., Ding, L., Huang, Q.S., Zhang, X.R., Yue, Y.H., Zhang, L.Y., 2015. Zircon U–Pb age and Hf isotopic compositions of Mesozoic granitoids in southern Qiangtang, Tibet: implications for the subduction of the Bangong-Nujiang Tethyan Ocean. Gondwana Res. http://dx.doi.org/10.1016/j.gr.2015.04.007.
Martinod, J., Husson, L., Roperch, P., Guillaume, B., Espurt, N., 2010. Horizontal subduction zones, convergence velocity and the building of the Andes. Earth Planet. Sci. Lett. 299, 299–309.
Middlemost, E.A.K., 1994. Naming materials in the magma/igneous rock system. Earth Sci. Rev. 37, 215–224.
Miller, C., Schuster, R., Klötzli, U., Frank, W., Purtscheller, F., 1999. Post-collisional potassic and ultrapotassic magmatism in SW Tibet: geochemical and Sr–Nd–Pb–O isotopic constraints for mantle source characteristics and petrogenesis. J. Petrol. 40 (9), 1399–1424.
Mo, X.X., Dong, G.C., Zhao, Z.D., Zhou, S., Wang, L.L., Qiu, R.Z., Zhang, F.Q., 2005. Spatial and temporal distribution and characteristics of granitoids in the Gangdese, Tibet and implication for crustal growth and evolution. Geol. J. China Univ. 11 (3), 281–290 (in Chinese with English abstract).
Murphy, J.B., Hynes, A.J., Johnston, S.T., Keppie, J.D., 2003. Reconstructing the ancestral Yellowstone plume from accreted seamounts and its relationship to flat-slab subduction. Tectonophysics 365, 185–194.
Pan G.T., Ding J., Yao D.S., Wang L.Q., 2004. Geological map of the Qinghai-Xizang (Tibet) plateau and adjacent areas (1:1500,000) and synopsis. Chengdu Cartographic Publishing House.
Peng T.P., Yang X.M., Chu H.L., Lin G.L., 2015., Major discovery on the ocean islands constitutive model and prospecting in Gerze County of the Bangong Lake-Nujiang River suture zone: according to 1: 50000 Gerze County (I45E021005) and other five regional geological maps in Tibet. 2(2): 12–23(in Chinese with English abstract).
Qu, X.M., Xin, H.B., 2006. Ages and tectonic environment of the Bangong Co porphyry copper belt in western Tibet, China. Geol. Bull. China 25 (7), 792–799 (in Chinese with English abstract).
Qu, X.M., Xin, H.B., Du, D.D., Chen, H., 2013. Magma source of the A-type granite and slab break-off in the middle segment of the Bangonghu-Nujiang suture, Tibet plateau. Acta Geol. Sin. 87 (6), 759–772 (in Chinese with English abstract).
Ramos, V.A., McNulty, B., 2002. Flat-slab subduction in Andes. J. S. Am. Earth Sci. 15, 1–2.
Richards, J.P., 2015. Tectonic, magmatic, and metallogenic evolution of the Tethyan orogen: from subduction to collision. Ore Geol. Rev. 70, 323–345.
Roger, F., Jolivet, M., Malavieille, J., 2008. Tectonic evolution of the Triassic fold belts of Tibet. Compt. Rendus Geosci. 340, 180–189.
Schütte, P., Chiaradia, M., Beate, B., 2010. Geodynamic controls on Tertiary arc magmatism in Ecuador: constraints from U–Pb zircon geochronology of Oligocene–Miocene intrusions and regional age distribution trends. Tectonophysics 489, 159–176.
Shand, S.J., 1943. Eruptive Rocks: Their Genesis, Composition, Classification, and Their Relation to Ore-Deposits With a Chapter on Meteorite. John Wiley & Sons, New York.
She, H.Q., Li, J.W., Ma, D.F., Li, G.M., Zhang, D.Q., Feng, C.Y., Qu, W.J., Pan, G.T., 2009. Molybdenite Re–Os and SHRIMP zircon U–Pb dating of Duobuza porphyry copper deposit in Tibet and its geological implications. Mineral Deposits 28 (6), 737–746 (in Chinese with English abstract).
Sun, S.S., McDonough, W.E., 1989. Chemical and isotopic systematics of oceanic basalts: implications for mantle composition and processes. In: Saunders, A.D., Norry, M.J. (Eds.), Magmatism in the Ocean Basins: Geological Society of London. Special Publication Vol. 42, pp. 313–345.
Tang, J.X., Sun, X.G., Ding, S., Wang, Q., Wang, Y.Y., 2014. Discovery of the epithermal deposit of Cu (Au–Ag) in the Duolong ore concentrating area, Tibet. Acta Geosci. Sin. 35 (1), 6–10 (in Chinese with English abstract).
Tibet Institute of Geological Survey, 2012, 1:250000 geological survey report of Gerze county, Tibet, Wuhan: China University of Geosciences Press (in Chinese).
Wang, J., Tan, F.W., Li, Y.L., Li, Y.T., Chen, M., Wang, C.S., Guo, Z.J., 2004. The potential of the oil and gas resources in major sedimentary basins on the Qinghai-Xizang (Tibet) Plateau. Geological Publishing House, pp. 1–329 (in Chinese).
Wang, W.L., Aitchison, J.C., Lo, C.H., Zeng, Q.G., 2008. Geochemistry and geochronology of the amphibolite blocks in ophiolitic me'langes along Bangong-Nujiang suture, central Tibet. J. Asian Earth Sci. 33, 122–138.
Wang, Z.H., Liu, Y.L., Liu, H.F., Guo, L.S., Zhang, J.S., Xu, K.F., 2012. Geochronology and geochemistry of the Bangpu Mo–Cu porphyry ore deposit, Tibet. Ore Geol. Rev. 46, 95–105.
Wei, G.J., Liang, X.R., Li, X.H., Liu, Y., 2002. Precise measurement of Sr isotopic composition of liquid and solid base using (LP)MC-ICPMS. Geochimica 31 (3), 295–299 (in Chinese with English abstract).
Xie, C.M., Li, C., Dong, Y.S., Wu, Y.W., Wang, M., Hu, P.Y., 2010. Gangmari-Juhuashan thrust nappe were discovered in central Qiangtang, northern Tibet, China. Geol. Bull. China 29 (12), 1857–1862 (in Chinese with English abstract).
Xin, H.B., Qu, X.M., Wang, R.J., Liu, H.F., Zhao, Y.Y., Huang, W., 2009. Geochemistry and Pb, Sr, Nd isotopic feature of ore-bearing porphyries in Bangong Lake porphyry copper belt, western Tibet. Mineral Deposits 28 (6), 785–792 (in Chinese with English abstract).
Yang, Z.M., Hou, Z.Q., White, N.C., Chang, Z.S., Li, Z.Q., Song, Y.C., 2009. Geology of the post-collisional porphyry copper–molybdenum deposit at Qulong, Tibet. Ore Geol. Rev. 36, 133–159.
Yang, Z.M., Lu, Y.J., Hou, Z.Q., Chang, Z.S., 2015. High-Mg diorite from Qulong in Southern Tibet: implications for the genesis of adakite-like intrusions and associated porphyry Cu deposits in Collisional Orogens. J. Petrol. 56 (2), 227–254.
Zhang, Y.X., 2007. Tectonic evolution of the middle-western Bangong-Nujiangsuture, Tibet. Supervisor: Prof. Zhang K.J., a Thesis Submitted for the Degree of Doctorate at the Graduate School of the Chinese Academy of Sciences, pp. 1–230 (in Chinese with English abstract).
Zhang, Z.M., Zhao, G.C., Santosh, M., Wang, J.L., Dong, X., Shen, K., 2010. Late Cretaceous charnockite with adakitic affinities from the Gangdese batholith, southeastern Tibet: evidence for Neo-Tethyan mid-ocean ridge subduction? Gondwana Res. 17, 615–631.
Zhang, Z., Geng, Q.R., Peng, Z.M., Cong, F., Guan, J.L., 2011. Geochemistry and geochronology of the Caima granites in the western part of the Bangong Lake-Nujiang metallogenic zone, Xizang. Sediment. Geol. Tethyan Geol. 31 (4), 86–96 (in Chinese with English abstract).
Zhang, Z.M., Dong, X., Santosh, M., Zhao, G.C., 2014. Metamorphism and tectonic evolution of the Lhasa terrane, Central Tibet. Gondwana Res. 25, 170–189.
Zhang, Z., Geng, Q.R., Peng, Z.M., Cong, F., Guan, J.L., 2015. Petrogenesis of Fuye pluton in Rutog, Tibet: zircon U–Pb dating and Hf isotopic constraints. Geol. Bull. China 34 (2/3), 262–273 (in Chinese with English abstract).
Zhao, Z.Z., Li, Y.T., Ye, H.F., Zhang, Y.W., 2001. Stratigraphy of the Qinghai-Tibet Plateau. Science Press, Beijing, pp. 1–542 (in Chinese).
Zhu, D.C., Mo, X.X., Niu, Y.L., Zhao, Z.D., Wang, L.Q., Pan, G.T., Wu, F.Y., 2009. Zircon U–Pb dating and in-situ Hf isotopic analysis of Permian peraluminous granite in the Lhasa terrane, southern Tibet: implications for Permian collisional orogeny and paleogeography. Tectonophysics 469, 48–60.
Zhu, D.C., Zhao, Z.D., Niu, Y.L., Dilek, Y., Mo, X.X., 2011a. Lhasa Terrane in southern Tibet came from Australia. Geology 39, 727–730.
Zhu, D.C., Zhao, Z.D., Niu, Y.L., Mo, X.X., Chung, S.L., Hou, Z.Q., Wang, L.Q., Wu, F.Y., 2011b. The Lhasa Terrane: record of a microcontinent and its histories of drift and growth. Earth Planet. Sci. Lett. 301, 241–255.
Zhu, X.P., Chen, H.A., Ma, D.F., Huang, H.X., Li, G.M., Li, Y.B., Li, Y.C., 2011c. Re–Os dating for the molybdenite from Bolong porphyry copper-gold deposit in Tibet,China and its geological significance. Acta Petrol. Sin. 27 (7), 2159–2164 (in Chinese with English abstract).
Zhu, X.P., Chen, H.A., Ma, D.F., Huang, H.X., Li, G.M., Wei, L.J., Liu, C.Q., 2012. Geology and alteration of the Duobuza porphyry copper-gold deposit in Tibet. Geol. Explor. 48 (2), 199–206 (in Chinese with English abstract).
Zhu, X.P., Chen, H.A., Ma, D.F., Huang, H.X., Li, G.M., Li, Y.B., Li, Y.C., Wei, L.J., Liu, C.Q., 2013. 40Ar/39Ar dating of hydrothermal K-feldspar and hydrothermal sericite from Bolong porphyry Cu–Au deposit in Tibet. Mineral Deposits 32 (5), 945–962 (in Chinese with English abstract).
Zhu, D.C., Li, S.M., Cawood, P.A., Wang, Q., Zhao, Z.D., Liu, S.A., Wang, L.Q., 2015a. Assembly of the Lhasa and Qiangtang terranes in central Tibet by divergent double subduction. Lithos http://dx.doi.org/10.1016/j.lithos.2015.06.023.
Zhu, X.P., Li, G.M., Chen, H.A., Ma, D.F., Huang, H.X., 2015b. Zircon U–Pb, molybdenite Re–Os and K-feldspar 40Ar/39Ar dating of the Bolong Porphyry Cu–Au deposit, Tibet, China. Resour. Geol. 65 (2), 122–135.